N80-14131

NASA CONTRACTOR REPORT 159192

OBLIQUE DETONATION WAVE RAMJET

RICHARD B. MORRISON

UNIVERSAL SYSTEMS, INC.
2341 JEFFERSON DAVIS HIGHWAY,
SUITE 820,
ARLINGTON, VA 22202

CONTRACT NAS1-15344.
JANUARY 1980

Original

NASA
National Aeronautics and
Space Administration

Langley Research Center
Hampton, Virginia 23665
AC 804 827-3966

NASA CONTRACTOR REPORT 159192

OBLIQUE DETONATION WAVE RAMJET

RICHARD B. MORRISON

UNIVERSAL SYSTEMS, INC.
2341 JEFFERSON DAVIS HIGHWAY,
SUITE 820,
ARLINGTON, VA 22202

CONTRACT NAS1-15344
JANUARY 1980

National Aeronautics and
Space Administration

Langley Research Center
Hampton, Virginia 23665
AC 804 827-3966

TABLE OF CONTENTS

LIST OF FIGURES

LIST OF TABLES

OBLIQUE DETONATION WAVE RAMJET

Richard B. Morrison
Universal Systems, Inc.

SUMMARY

Two conceptual designs of the oblique detonation wave ramjet are presented and the performance evaluated for stoichiometric hydrogen-air equivalence ratios of $\phi = {}^{1}/_{3}, {}^{2}/_{3}$ and 1 for a range of flight Mach numbers from 6 to 10.

1.0 Introduction

Interest in ramjet propulsion began toward the end of World War II at a time when the turbojet was being accepted as an effective means of obtaining higher flight speeds. In this time period it was also felt that ramjet propulsion would be a next step for attaining still higher flight speeds. Ramjets were also envisioned as vehicles for delivering warheads over intercontinental distances either by cruise or by skip flight trajectories. All of these proposed techniques involved subsonic combustion for supersonic vehicles operating at low supersonic speeds.

The competition of the rocket and the ramjet for payloads to be delivered over intercontinental distances was awarded to the rocket in the 1950's and interest in subsonic combustion ramjet propulsion waned to very low levels. Interest in "supersonic combustion ramjets" and "standing detonation wave ramjets" increased during this period. Numerous ramjet configurations and techniques were offered that utilized these latter concepts, however, only one persisted and survived, that of the diffusive burning scramjet. With this singular exception it appears most of the interest in hypersonic airbreathing propulsion ceased in the 1965 to 1970 time period.

The use of oblique detonation waves is a more recent consideration for use in ramjets that operate at hypersonic speeds. This concept differs markedly from the diffusive burning scramjet.

The diffusive burning scramjet compression process is carried out to the high pressures and the high temperatures required for diffusive burning in the combustion section of the ramjet i.e., diffusion from a flight Mach number of 6 to 8 to a combustion chamber Mach number of 2 to 2.5.

The compression process of the oblique detonation wave ramjet is moderate and carried out to relatively low pressures and temperatures. The shock component of the detonation process supplies the additional large compression as well as the corresponding high temperatures required for the rapid combustion portion of the detonative process.

The above concept, having received little attention in the past, was analyzed and its position in the flight regime of airbreathing propulsors delineated. The results of that study were presented in the final report to NASA Langley Research Center, Contract No. NAS-1-14771, January 1978.

In the above report the potential performance of oblique detonation wave ramjets was analyzed in terms of multi-shock diffusion, oblique Chapman-Jouguet detonation waves and heat release with the results reported in terms of thrust coefficients and specific impulses for a range of flight Mach numbers 6 to 16.

It was concluded that the oblique detonation wave ramjet offers great potential as an airbreathing propulsor to extend the useful range of ramjet flight Mach numbers from 6 to 16 and above.

Specific impulses and thrust coefficients that would be attainable in the above flight range would exceed 70 percent of ideal.

Multi-shock diffusers offer much promise as the means of tailoring a simple configuration to meet requirements for variable speed and variable fuel-air ratios. Two or three oblique shock configurations appear to represent the best compromise between simplicity and performance for fixed geometry ramjets.

Stable operation of the detonation wave ramjet exists at flight Mach numbers in excess of 6.

The shock portion of the detonation wave constitutes a most important part of the compression process by alleviating demands upon the diffuser and providing a high temperature for ignition of the mixture. Unlike diffusive supersonic combustion, chemical reaction is promoted in very short distances.

Uncertainty of detonation limits at elevated temperatures was judged the largest unknown parameter influencing the performance.

Patch[1] has shown that a Chapman-Jouguent detonation will occur when the non-equilibrium temperatures immediately behind the leading shock are approximately 1300^0K to 1400^0K. J. A. Nicholls, at the University of Michigan, established a standing normal hydrogen-air detonation wave in a free jet "shock-bottle" configuration possessing a stagnation

temperature of approximately 1500°K. This would conform to Patch's criterion.

The spontaneous ignition temperature for hydrogen-air mixtures (NACA Report 1383) is approximately 900°K which indicates an upper limit of static temperatures wherein detonation can occur (i.e., an elevated temperature detonation limit). Inasmuch as the static temperatures in advance of the detonation front for the present engine are significantly lower than this, and the stagnation temperatures are considerably higher than Patch's requirement of 1300 to 1400K, it may be expected that the uncertainty of elevated temperature detonation limits would be of no particular concern.

To determine the research that had been carried out on oblique detonation wave ramjets and to identify any related and overlooked airbreathing propulsion research a thorough literature search was conducted through the Defense Documentation Center (DDC), the Navy intelligence systems, and other government agencies.

A partically annotated bibliography of the most useful documentation resulting from the above literature search was provided NASA Langley as a separate document independent of the final report.

The results of the above study determine that further analytical research should be directed toward a conceptual design and performance estimate of an oblique detonation wave ramjet engine in regard to the following items:

1. Determine off-design point multi-shock diffuser performance to delineate the flight Mach number range for fixed geometries.

2. Determine geometric implications of diffuser performance from Item 1, to include effects of nozzle area ratios and incomplete nozzle expansion pressure ratios upon the overall ramjet performance.

3. Estimate the effects of premixed fuel injector losses on diffuser performance, including associated shock and mixing losses.

4. Prepare a conceptual design of a hypersonic ramjet utilizing the oblique detonation wave as the propulsion combustion process, and compare performance and takeover speed with that of a scramjet, where both engines are of the same assumed idealized concept with respect to types of losses included or neglected.

5. Make an estimate of the effect of dissociation and incomplete recombination of the products of detonation on the engine performance.

In order to most effectively carry out this study for off-design point multi-shock diffuser performance, along with the associated geometric implications incurred, a set of oblique shock curves was generated and utilized.

The "Evaluation of the Oblique Detonation Wave Ramjet" (Contract No. NAS-1-14771) considered only the use of oblique Chapman-Jouguet detonations with "design point conditions" at each flight Mach number; i.e., the implication of a completely "rubber" ramjet.

Fixed geometry ramjets, operating at higher than design point Mach numbers would force strong detonation to occur in the ramjet combustor. Accordingly then a set of oblique strong detonation wave curves was generated and utilized.

2.0 Diffuser Configuration Optimizations and Compromises

2.1 General Considerations

The optimization of multi-shock diffuser configurations requires near-optimum design point configurations that are compromised to meet the following considerations:

- Minimized spillover at flight Mach numbers below the design Mach number. Spillover adversely influences takeover Mach numbers
- Minimized ingestion of the stronger oblique shock flows that result from the intersection of the weaker oblique shocks generated in the diffuser.
- The above shock ingestion is the prime influence that limits performance at flight Mach numbers above the design Mach number
- Minimized Mach numbers for fuel injection. These losses are appreciable for lean mixtures
- Minimized Mach numbers for fuel injection. These losses can be excessive for rich mixtures.
- Provision of the proper flow geometry to the oblique detonation wave

2.1.1 Spillage Losses

Spillage losses can be evaluated in terms of their effects upon various performance parameters of the component ramjets elements, i.e., the diffuser itself, the fuel injection system, the combustion chamber, etc. For the purposes of evaluation of overall thrust, the effect of the spillage upon the overall thrust coefficient is most pertinent.

The equation for the overall thrust coefficient, C_T, is derived from the conservation equations in terms of the entrance and exit Mach numbers. For a ramjet that exhausts to atmospheric pressure:

$$C_T \equiv \frac{F_x}{\dot{m}_a V_1} = \left(1 + \frac{\dot{m}_f}{\dot{m}}\right) \frac{M_{ex}}{M_{in}} \left[1 + \frac{Q}{C_p T_{oin}}\right]^{\frac{1}{2}} \left[\frac{1 + \frac{\gamma-1}{2} M_{in}^2}{1 + \frac{\gamma-1}{2} M_{ex}^2}\right]^{\frac{1}{2}} - 1 \qquad \text{---2.1.1.1}$$

F_x = Thrust

$\dot{m}_a$ = Mass flow of intake air

$\dot{m}_f$ = Mass flow of fuel

V_1 = Free stream velocity

γ = Ratio of specific heats

M_{in} = Entrance Mach number

M_{ex} = Exit Mach number

Q = Heat added

C_T = Specific heat at constant pressure

T_{oin} = Free stream stagnation temperature

The equivalent expression for C_p in terms of stagnation pressure loss is:

$$C_T = \left[1 + \frac{\dot{m}_f}{\dot{m}_a}\right]\left[\frac{\left(\frac{p_{oex}}{p_{in}}\right)^{\frac{\gamma-1}{\gamma}}}{\left(\frac{p_{oin}}{p_{in}}\right)^{\frac{\gamma-1}{\gamma}}}\right]^{\frac{1}{2}} \left(1 + \frac{Q}{C_p T_{oin}}\right)^{\frac{1}{2}} \left(\frac{p_{oin}}{p_{oex}}\right)^{\frac{\gamma-1}{2\gamma}} - 1 \qquad \text{----2.1.1.2}$$

Where:

p_{in} = Free stream static pressure

p_{oin} = Free stream stagnation pressure

p_{ex} = Exhaust static pressure

p_{oex} = Exhaust stagnation pressure

Equations 2.1.1.1 and 2.1.1.2 which define the thrust coefficient in terms of the captured incoming momentum, can be corrected for air spillage in the same manner as the correction for fuel flow, $\dot{m}_f$. This results in an expression in the form of:

$$C_{TSP} = C_{TOSP}\left(1 - \frac{\Delta\dot{m}_a}{\dot{m}_a}\right) \qquad \text{----------2.1.1.3}$$

Where:

C_{TSP} = Thrust coefficient with spillage

C_{TOSP} = Thrust coefficient with no spillage or thrust coefficient associated with all the airflow passing internally through the ramjet

$\dot{m}_a$ = Mass flow of intake air including spillage air

$\Delta\dot{m}_a$ = Mass flow of spillage air

Determination of $\frac{\dot{\Delta m}_a}{\dot{m}_a}$ is made from the flow geometry by tracing back the parting streamline from the diffuser lip to free stream conditions and identifying that portion of airflow that is spilled.

The degradation of the thrust coefficient from spillage losses can be interpreted in terms of an equivalent diffuser stagnation pressure or kinetic energy loss from Equation 2.1.1.2 or the equivalent C_T charts.

2.1.2 Oblique Shock Diffuser Curves.

The equations for oblique waves are:

$$\tan\Theta = \frac{\frac{2}{\gamma+1}\left(1-\frac{1}{M_1^2\sin^2\beta}\right)\tan\beta}{1+\tan^2\beta\left[1-\frac{2}{\gamma+1}\left(1-\frac{1}{M_1^2\sin^2\beta}\right)\right]} \qquad \text{--------2.1.2.1}$$

and

$$M_2\sin(\beta-\Theta) = \sqrt{\frac{(\gamma-1)(M_1^2\sin^2\beta-1)+(\gamma+1)}{2\gamma(M_1^2\sin^2\beta-1)+(\gamma+1)}} \qquad \text{-----2.1.2.2}$$

Where

F = Wave classification number

M_1 = Free stream Mach number

M_2 = Mach number behind oblique shock

Θ = Wedge angle

β = Oblique shock wave angle

γ = Ratio of specific heats

Graphs for these equations may be found in NACA Report 1135, however, the format does not readily lend itself to rapid and accurate multi-shock diffuser analysis. Therefore Figure 2.1.2.1 (page 11) was prepared utilizing Equations 2.1.2.1 and 2.1.1.1 where the prime independent variable, θ and M_1 form the coordinate axes and the dependent variable, β, M_2 and $M_1 \sin \beta = M_{1n}$, are graphed.

It is noted that the thermodynamic state changes that take place across oblique shocks are a function only of M_{1n}, hence:

$$\frac{p}{p} = 1 + \frac{2\gamma}{\gamma+1} (M_1n^2 - 1) \qquad \text{----------2.1.2.3}$$

$$\frac{\rho_2}{\rho_1} = \frac{1}{1 - \frac{2}{\gamma+1}\left(\frac{(M_1n^2-1)}{M_1n^2}\right)} \qquad \text{----------2.1.2.4}$$

$$\frac{T_2}{T_1} = \left\{1 + \frac{2\gamma}{\gamma+1} (M_1n^2-1)\right\}\left\{1 - \frac{2}{\gamma+1} \frac{(M_1n^2-1)}{M_1n^2}\right\} \qquad \text{---2.1.2.5}$$

$$\frac{p_{02}}{p_{01}} = \left\{1 + \frac{2\gamma}{\gamma+1} (M_1n^2-1\right\}\left\{\frac{1 + \frac{\gamma-1}{2} M_2^2}{1 + \frac{\gamma-1}{2} M_1^2}\right\}^{\frac{\gamma}{\gamma-1}} \qquad \text{---2.1.2.6}$$

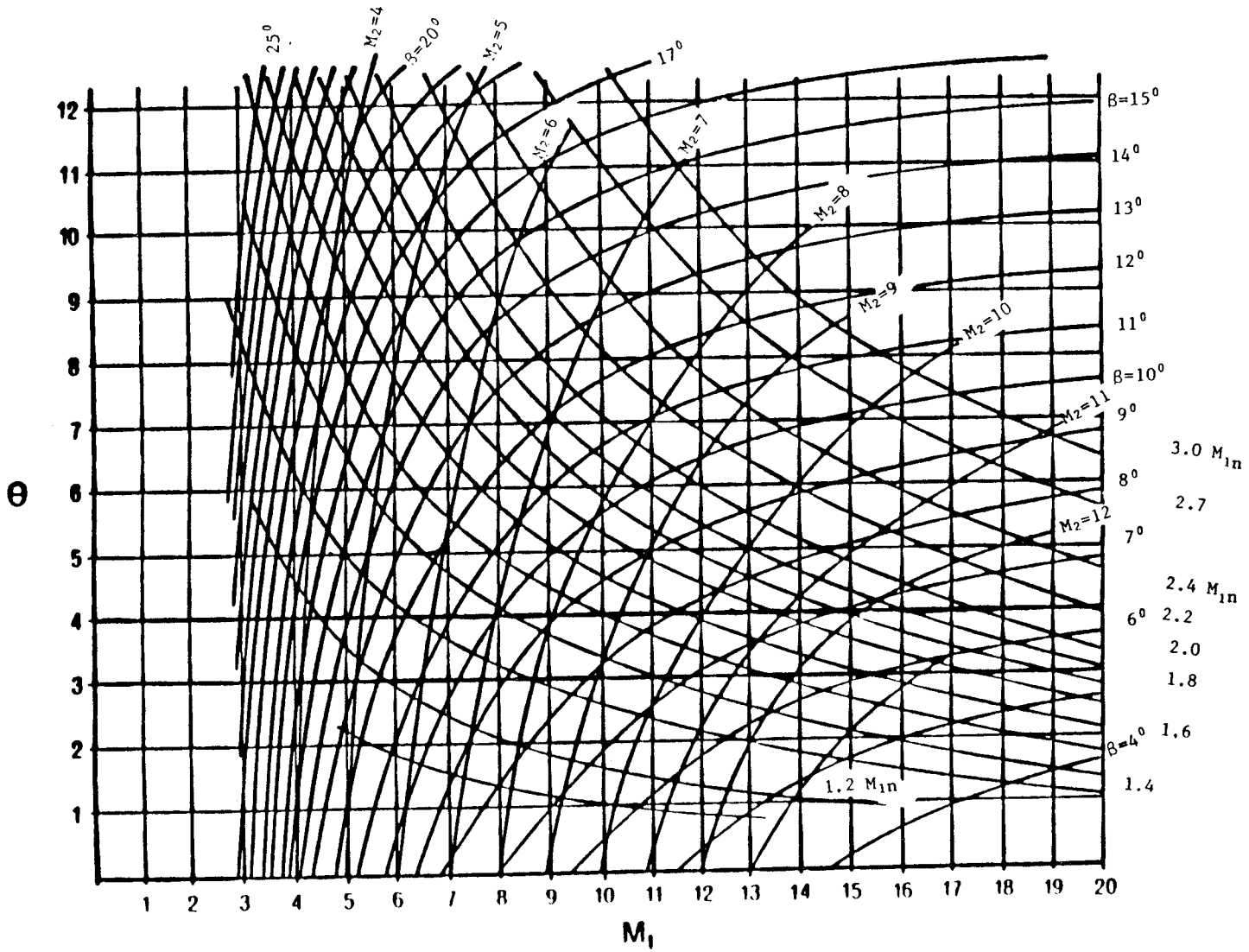

Figure 2.1.2.1 Oblique Shock Wave Properties

Where:

Subscript $_1$ denotes conditions upstream of the oblique shock wave. Subscript $_2$ denotes conditions downstream of the oblique shock wave and subscript $_0$ donotes stagnation conditions. No subscript denotes static conditions.

p = Pressure

T = Temperature

ρ = Density

Figure 2.1.2.1 can be utilized for ramjet analysis in a manner that is similar to that of a "compresser map" for turbojet analysis. For example along lines of constant M_{1n} the compression efficiency is constant.

2.2 Reflected Shock Diffuser

The reflected multi-shock diffuser represents the least complex geometric configuration that is amendable to efficient off-design point diffuser performance. Consideration must be given, however, to several factors, i.e.:

- The flow angle to the combustion chamber
- The influence of a constant deflection angle for each oblique shock. Ideally the deflection angle should be increased for each succeeding oblique shock by an amount that would keep M_{1n}, in Mach number normal to the wave, constant (M_{1n} = Mach Number Normal)
- The overall length of the forebody which is to be added to the internal dimensions

- The off-design point operation at low flight Mach numbers with spillover
- High speed operation with flow ingestion

A design Mach number of 8 has been chosen as the compromise between low takeover speeds and good high speed performance. At this Mach number a wedge angle of 5^0, which produces an $M_{1_n} = 1.5$, was selected as the compromise between excessive spillover at low speeds and reduced performance at high speeds.

Figure 2.2.1, 2.2.2, and 2.2.3 are the series of diffuser inlet designs for a design Mach number of 8 wherein the spillage and lip intersections are shown for a range of flight Mach numbers of 4 to 14.

It is noted that small wedge angles, which reduce spillage at low flight Mach numbers, dramatically increase the lip intersection distance, at high Mach numbers. This in turn, greatly increases the internal dimensions of the diffuser where the reflected oblique shocks occur.

Large wedge angles result in excessive spillover and compressed internal dimensions. A moderate wedge angle, circa 5 to 6, appears to be the best compromise.

Figure 2.2.4 shows the internal shock reflection geometry for a 5^0 wedge/ramp angles for a range of flight Mach numbers of $M_1 = 4$ to 14, and a design Mach number of 8.

At this design Mach number of 8 the second reflected

$\Theta=3^0$ $M_{design}=8$

SPILLAGE AND LIP INTERSECTION

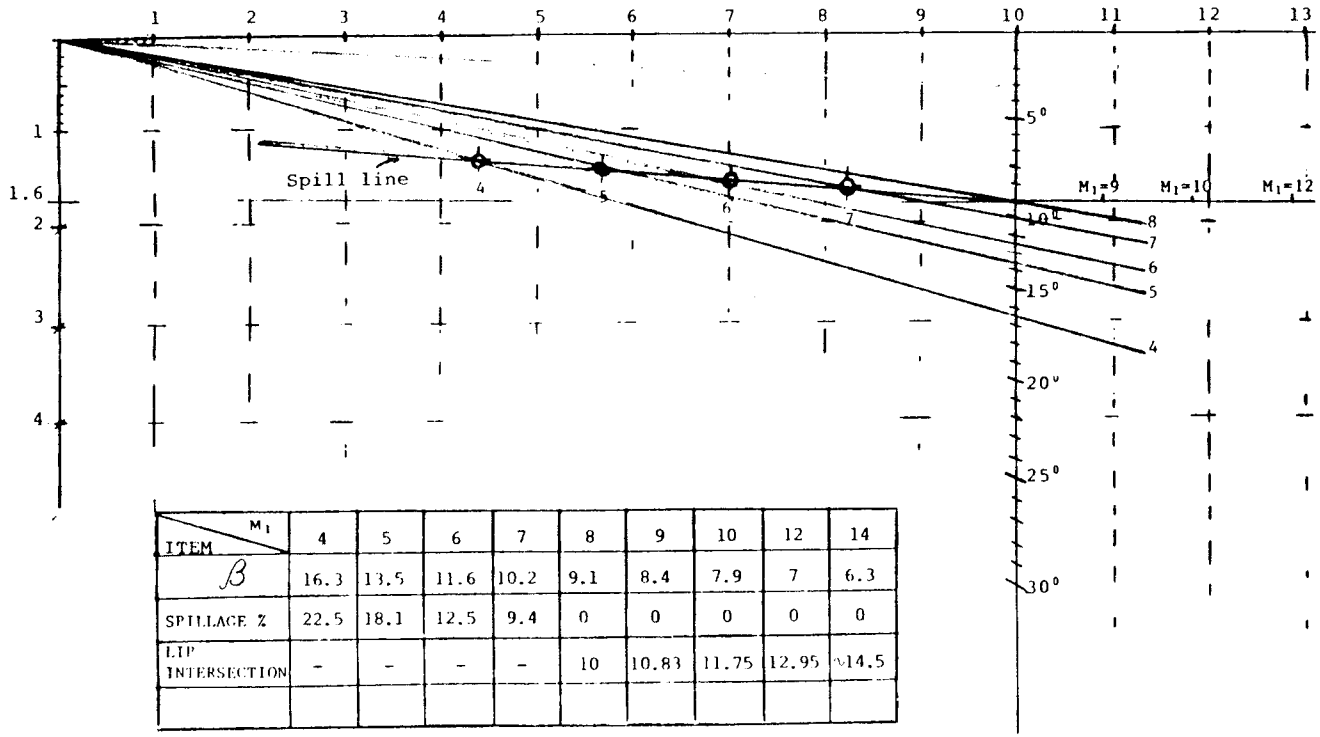

ITEM \ M_1	4	5	6	7	8	9	10	12	14
β	16.3	13.5	11.6	10.2	9.1	8.4	7.9	7	6.3
SPILLAGE %	22.5	18.1	12.5	9.4	0	0	0	0	0
LIP INTERSECTION	-	-	-	-	10	10.83	11.75	12.95	~14.5

Figure 2.2.1 Diffuser Design for $\Theta = 3^0$ $M_{design} = 8$

$\Theta = 5^0$ $M_{design} = 8$

SPILLAGE AND LIP INTERSECTION

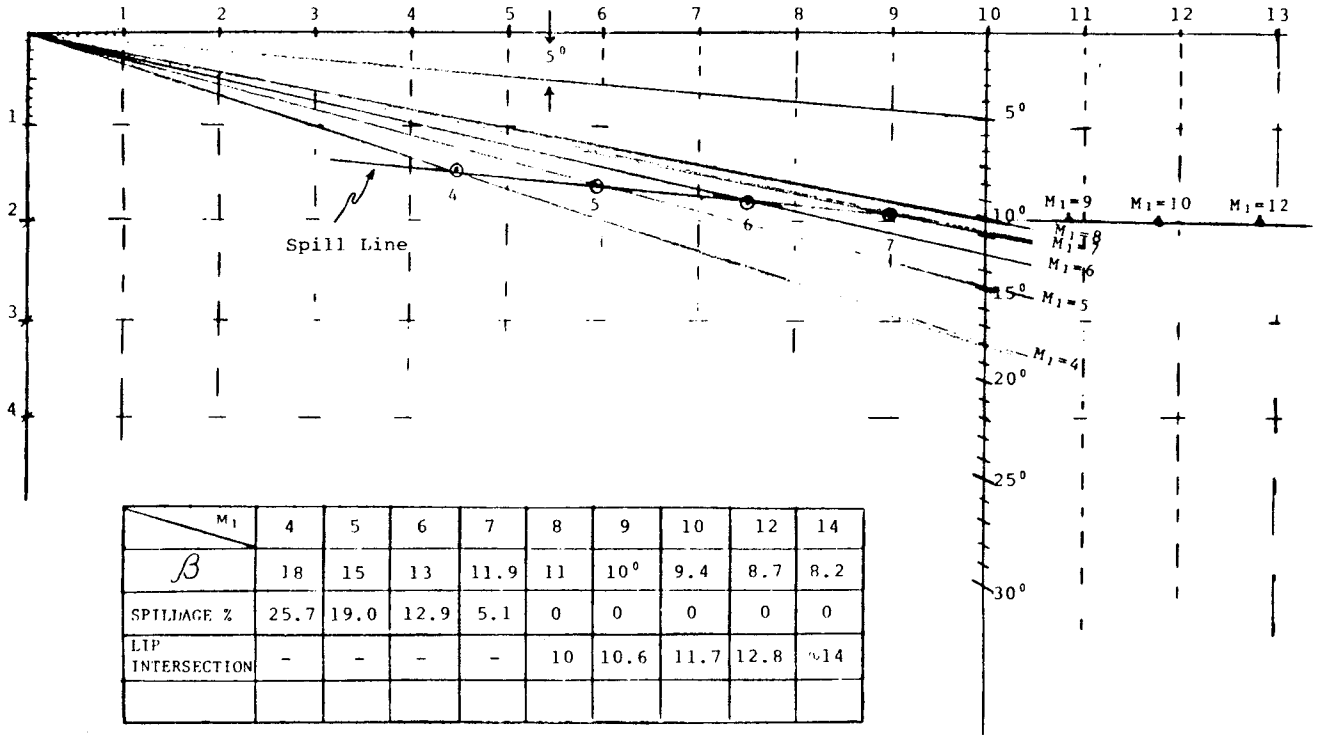

M_1	4	5	6	7	8	9	10	12	14
β	18	15	13	11.9	11	10°	9.4	8.7	8.2
SPILLAGE %	25.7	19.0	12.9	5.1	0	0	0	0	0
LIP INTERSECTION	-	-	-	-	10	10.6	11.7	12.8	≈14

Figure 2.2.2. Diffuser Design for $\Theta = 5^0$ $M_{design} = 8$

$\Theta=7^0$ $M_{design}=8$

SPILLAGE AND LIP INTERSECTION

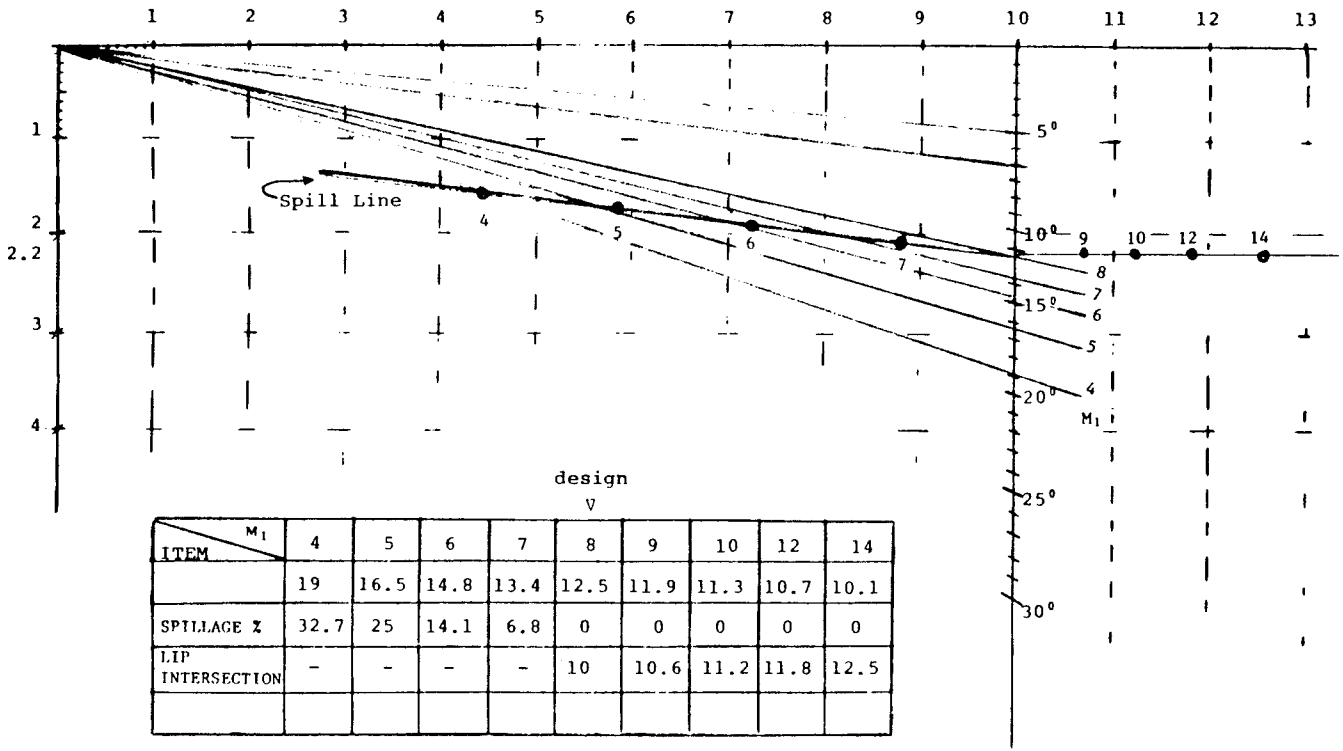

ITEM \ M_1	4	5	6	7	8	9	10	12	14
	19	16.5	14.8	13.4	12.5	11.9	11.3	10.7	10.1
SPILLAGE %	32.7	25	14.1	6.8	0	0	0	0	0
LIP INTERSECTION	-	-	-	-	10	10.6	11.2	11.8	12.5

Figure 2.2.3 Diffuser Design for $\Theta = 7^0$ $M_{design} = 8$

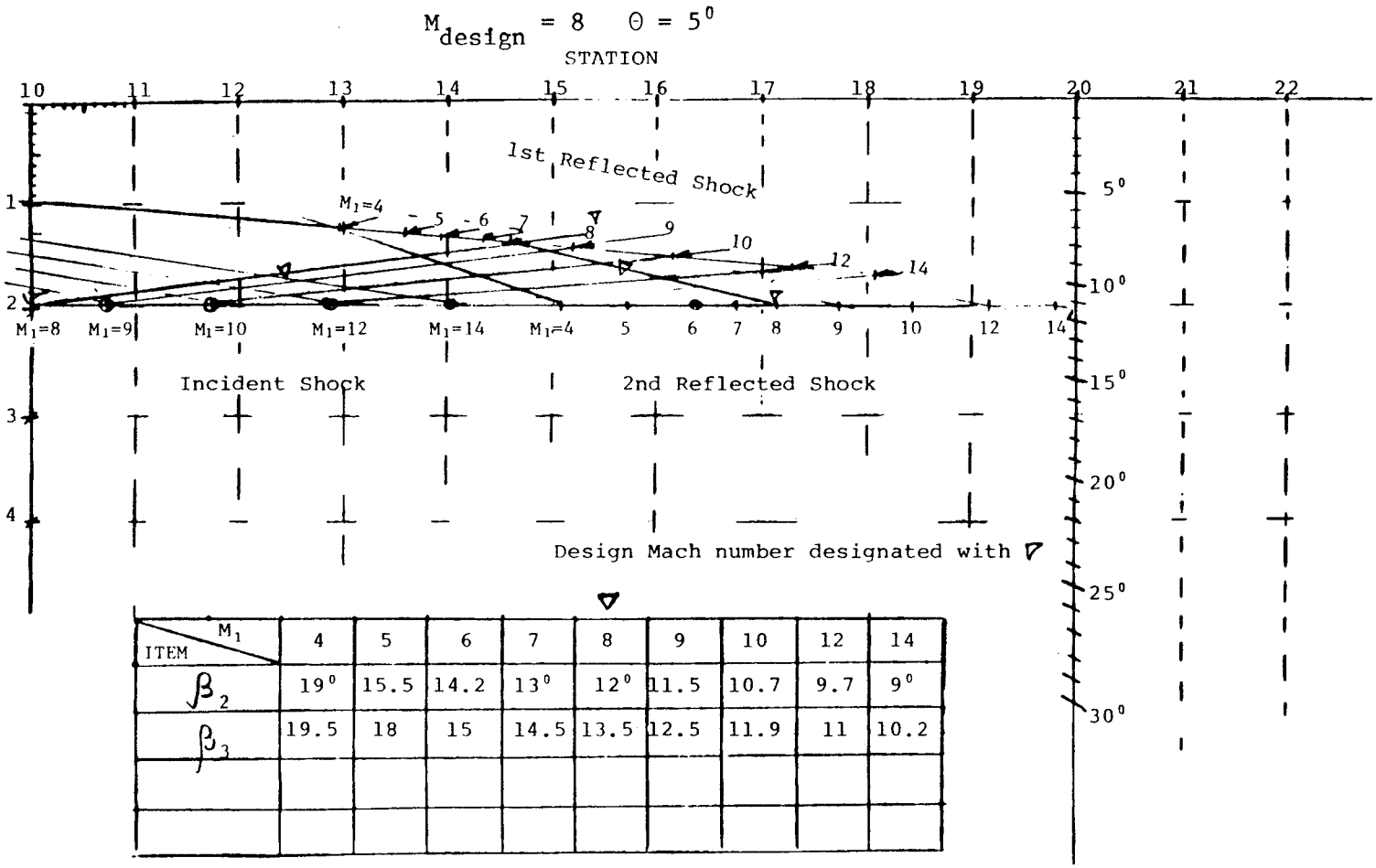

ITEM \ M_1	4	5	6	7	8	9	10	12	14
β_2	19°	15.5	14.2	13°	12°	11.5	10.7	9.7	9°
β_3	19.5	18	15	14.5	13.5	12.5	11.9	11	10.2

Figure 2.2.4 Internal Shock Geometry for $\Theta = 5^0$ $M_{design} = 8$

intersects the diffuser lip at station 17.15 and represents the design point location for the initiation of the oblique detonation wave. Fuel injection would be employed upstream from this location.

The wall intersection with the second reflected shock for $M_1 = M_{des}$ (Design Mach Number) moves forward as shown. This forward movement is small for $M_1 = 6$, the approximate takeover speed of the oblique detonation wave ramjet.

At flight Mach numbers of $M_1 > M_{des}$ the wall intersection with second reflected shock moves rearward rapidly, this in turn, leads to a deteriorated performance of high flight Mach numbers.

It may be concluded that a fixed geometry reflected shock diffuser, designed for $M_1 = 8$, would accommodate a takeover speed of $M_1 = 6$ and provide suitable performance for high speed flight of $M_1 = 12$ to 14.

2.3 Non-Reflected Multi-Shock Diffuser

The non-reflected multi-shock diffuser, unlike the reflected shock diffuser which utilizes constant deflection anlges, allows for a selection of deflection angles to accomplish more efficient compression than is provided by the reflected shock diffuser. This corresponds, in Figure 2.1.2.1, to follow a constant efficiency line i.e., a M_{1_n} = One of the Constant Lines. At the design point Mach

number, diffuser efficiencies are high, forebody lengths shortened, and ingested shocks dispensed with.

There are several other factors, however, that must be considered which are concerned with off-design point operation, i.e.:

- The flow angle to and location of the combustion chamber
- Off-design point operation at low Mach numbers with spillover
- Off-design point operation at high Mach numbers with shock intersections above and in front of the diffuser lip

A design Mach number of 8 was chosen for a first deflection angle of 5^0 and a second angle of 6^0, this closely corresponding to $M_{1_n} = 1.5$ for each shock.

Figure 2.3.1 shows the diffuser geometric shape and its properties when operated at other than design point conditions. It is noted that spillage losses are greater than those for the reflected shock diffuser. At a takeover Mach number of 6, spillage is 19 percent as compared to the reflected shock diffuser's 12.9 percent.

At Mach numbers in excess of design, shock intersections occur in advance of and above the diffuser lip. Figure 2.3.2 shows the resulting shock geometry. The normal component of the Mach number for Shock no. 3 is large with the accompanying high stagnation pressure losses.

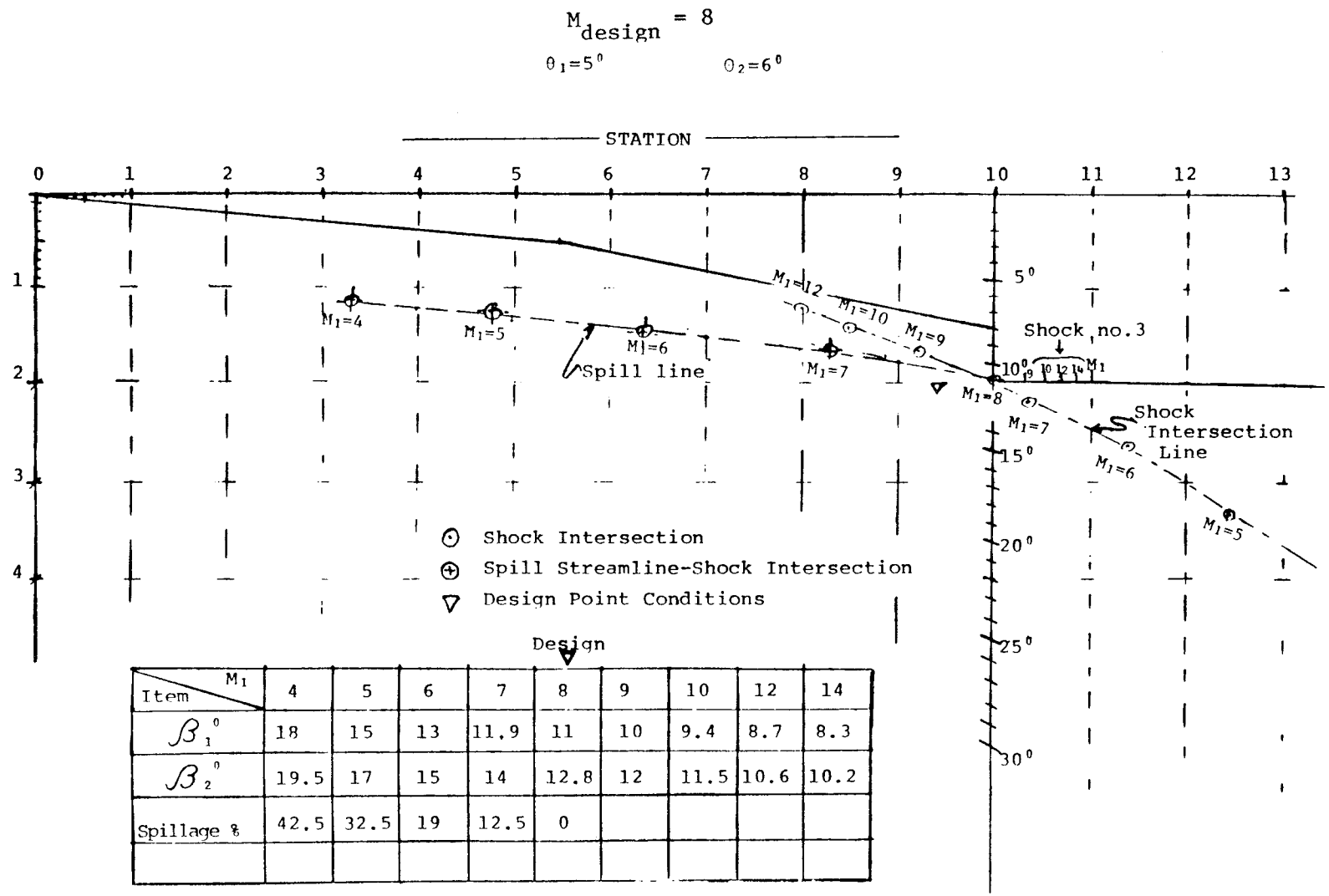

Item \ M_1	4	5	6	7	8	9	10	12	14
β_1^0	18	15	13	11.9	11	10	9.4	8.7	8.3
β_2^0	19.5	17	15	14	12.8	12	11.5	10.6	10.2
Spillage %	42.5	32.5	19	12.5	0				

Figure 2.3.1 Diffuser Design for θ_1=5°, θ_2=6°, M_{design}=8

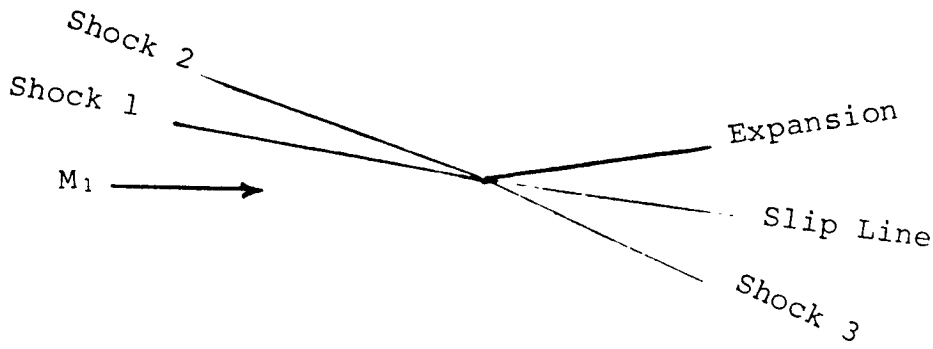

Figure 2.3.2 Intersection Oblique Shock Geometry

At $M_1 = 10$, $M_{1n} \simeq 2.7$. This is to be compared to Shock no. 1 with $M_{1n} \simeq 1.55$ and Shock no. 2, with $M_{1n} \simeq 1.5$ which remained close to the design $M_{1n} = 1.5$. The stagnation pressure ratio losses for Shocks no. 1 and no. 2 are approximately 0.83 as compared to Shock no. 3 of approximately 0.4.

The intersection of Shock no. 3 with the diffuser lip as shown in Figure 2.3.1 was estimated, for its most rearward location, by assuming a flow deflection equal to that of Shocks no. 1 and no. 2 of 11^0. The exact solution is found by adjusting the slip line angle to match the static pressure across the slip line. For this $M_1 = 10$ example, Shocks no. 1 and 2 possess a $M_{1n} \simeq 1.55$ resulting in a compression ratio of approximately 9. Shock no.3 possesses a $M_{1n} \simeq 2.7$ resulting in a compression ratio of approximately 8. A one degree increase in the Shock no. 3 deflection angle to 12^0 results in a compression ratio of approximately 9, indicating

a correction to the $M_1 = 10$ point in Figure 2.3.1 moving it to the location of the $M_1 = 9$ point. There is very little Shock no. 3 travel for this configuration, the shock lip intersection remaining between station 10 and 11 for flight Mach numbers up to $M_1 = 14$.

The effects of wedge angle upon shock geometry and diffuser performance are shown in Figure 2.3.3 and 2.3.4. Smaller wedge angles ameliorate spillage losses at small flight Mach numbers and increase the ingested distance of Shock no. 3.

Figure 2.3.5 shows the effects of increasing the design Mach number to 10. Spillage is greatly increased at low flight Mach numbers and the Shock no. 3 lip intersection distance is shortened at high flight Mach numbers.

It is concluded that a fixed geometry, non-reflecting multiple shock diffuser designed for $M_1 = 8$ with $\theta_1 = 5^0$ and $\theta_2 = 6^0$ would accommodate a takeover speed of $M_1 = 7$ and provide suitable performance to $M_1 = 10$ to 12 and possibly higher.

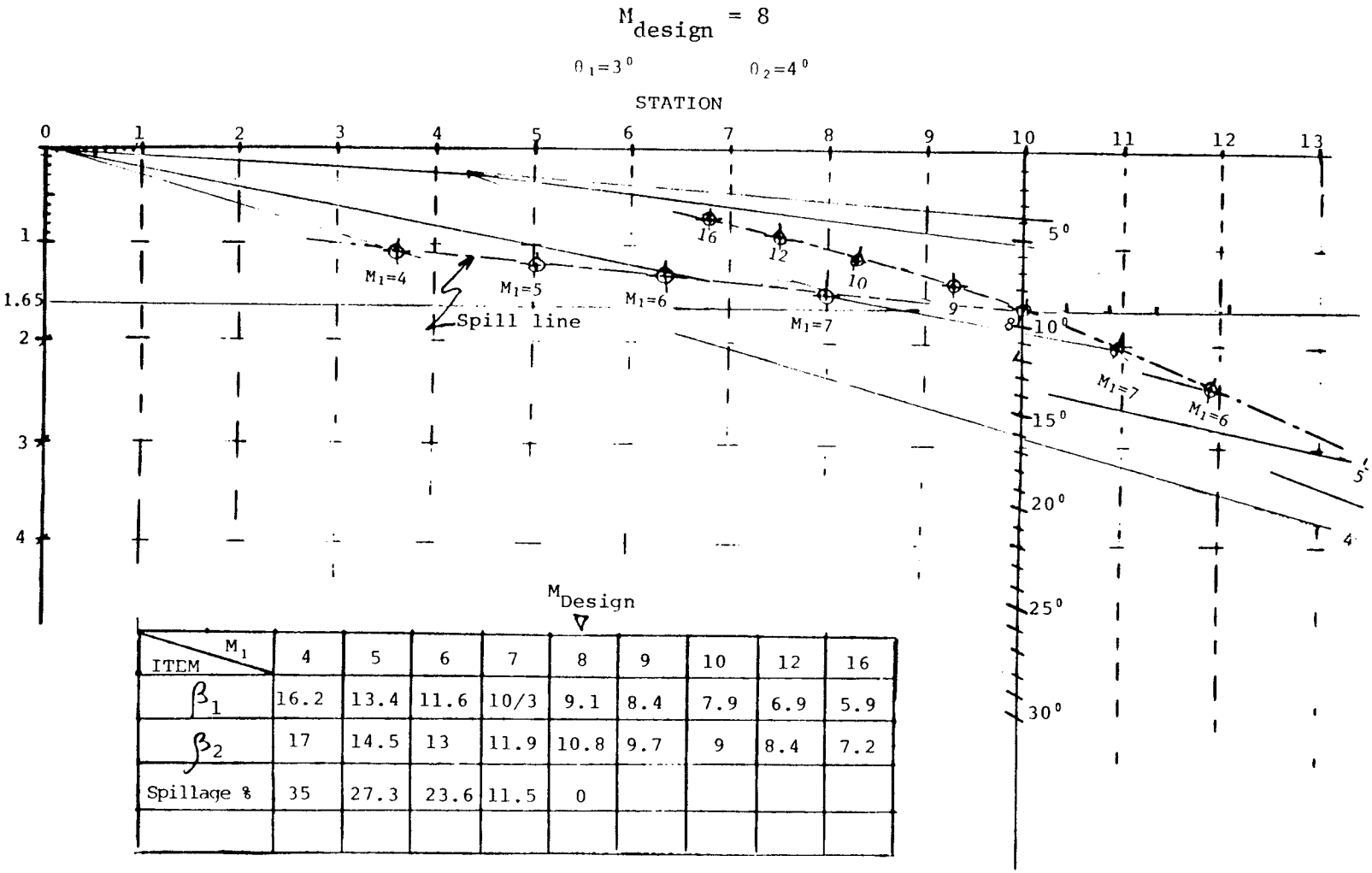

ITEM \ M_1	4	5	6	7	8	9	10	12	16
β_1	16.2	13.4	11.6	10/3	9.1	8.4	7.9	6.9	5.9
β_2	17	14.5	13	11.9	10.8	9.7	9	8.4	7.2
Spillage %	35	27.3	23.6	11.5	0				

Figure 2.3.3 Diffuser Design for θ_1 = 3° θ_2 = 4° M_{design} = 8

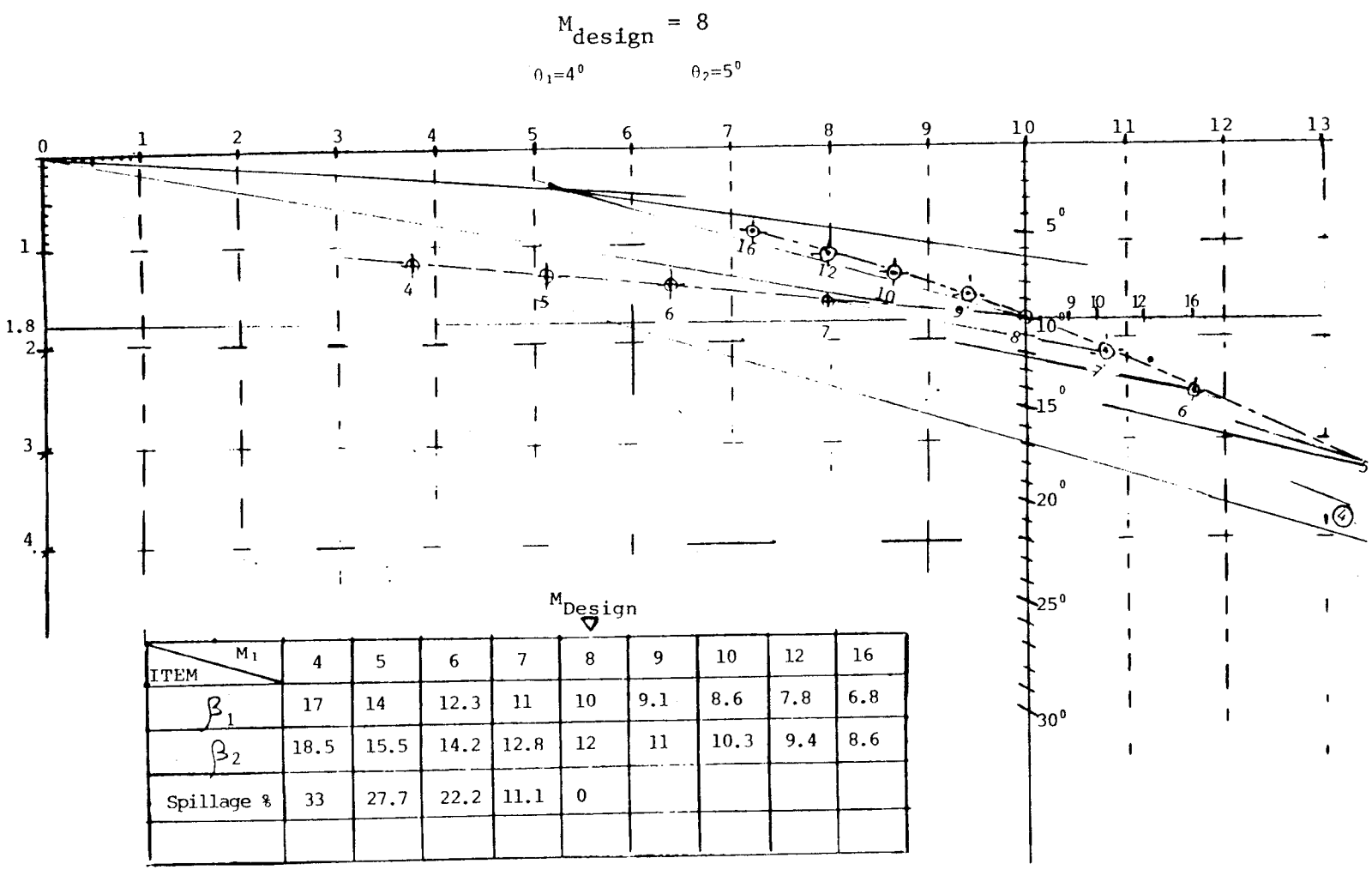

ITEM \ M_1	4	5	6	7	8	9	10	12	16
β_1	17	14	12.3	11	10	9.1	8.6	7.8	6.8
β_2	18.5	15.5	14.2	12.8	12	11	10.3	9.4	8.6
Spillage %	33	27.7	22.2	11.1	0				

Figure 2.3.4 Diffuser Design for $\theta_1 = 4^0$, $\theta_2 = 5^0$ $M_{design} = 8$

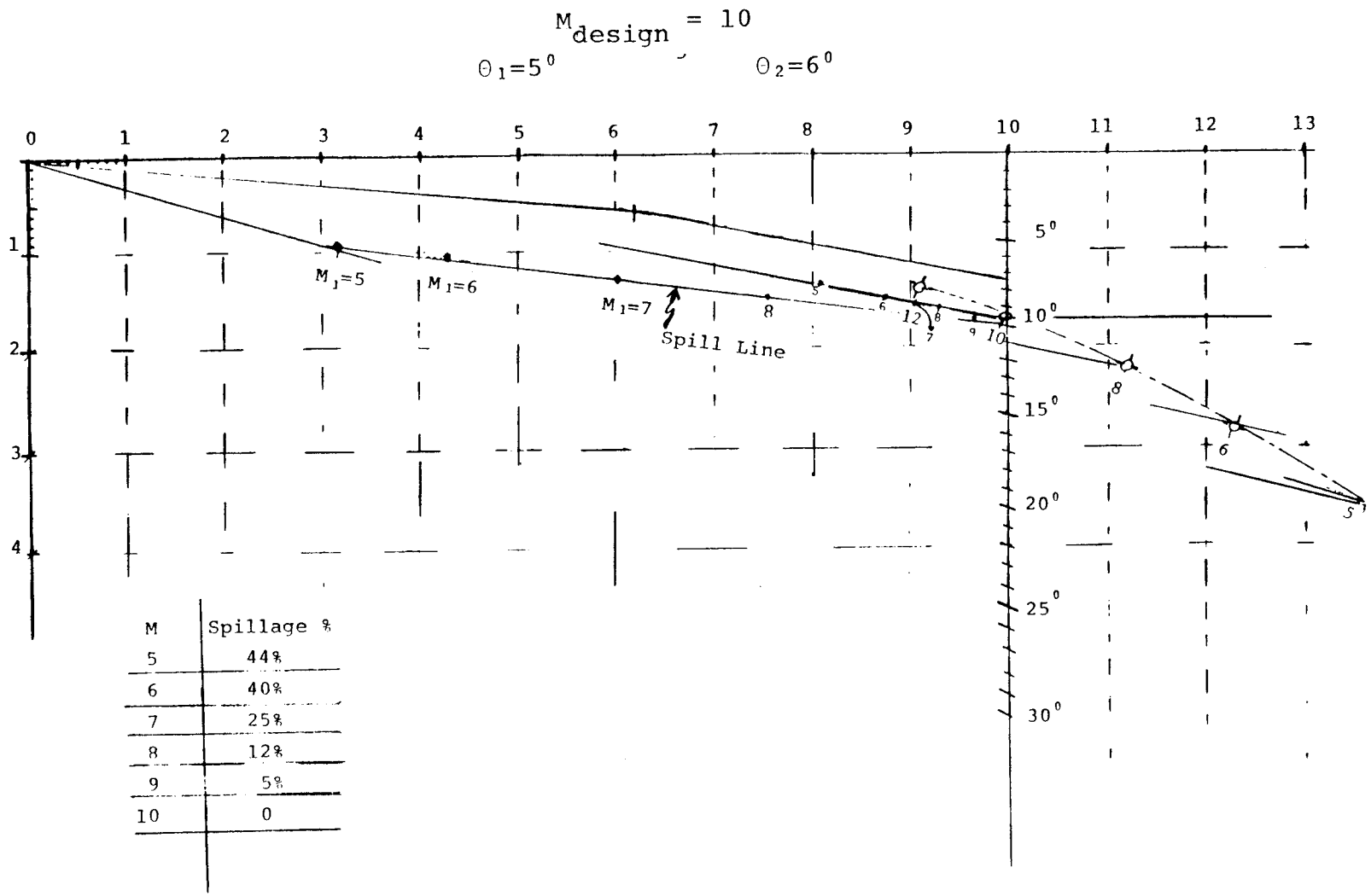

Figure 2.3.5 Diffuser Design for $\theta_1 = 5^0$, $\theta_2 = 6^0$ $M_{design} = 10$

3.0 Fuel Injection Losses

3.1 General Considerations

The injection of fuel into low speed airstreams such as encountered in engine carburetion or turbojet combustors constitutes little loss to overall system performance. Even distribution of the fuel throughout the desired combustion zone is the only major concern of such design.

The subsonic combustion ramjet, although primarily concerned with even fuel distribution throughout the combustion zone, is also very much concerned with flame holders and the ability to operate at lean mixture ratios. Losses in this case are more associated with flame holding techniques than with the fuel injection technique. Stream velocities are usually relatively low, in the order of 30 to 50 meters per second, and therefore require low fuel injection pressures to match airstream velocities.

The supersonic diffusive burning scramjet, however, with combustion at stream Mach numbers in the vicinity of 2 requires that fuel injection be accomplished with the following exacting considerations:

- Even fuel distribution provided throughout the airstream in extremely short time periods
- Injection at high pressures to provide penetration as well as a downstream component of fuel velocity to alleviate excessive losses from shocks and associated flow phenomena

The oblique detonation wave ramjet, in turn, with combustion taking place at Mach numbers in the range of 4 to 7, is severely penalized by fuel injection losses.

3.2 Fuel Injection Momentum Loss Analysis

Fuel injection losses can be estimated from momentum considerations if the following assumptions are made (see Figure 3.2.1):

- A constant pressure process exists within the mixing zone
- The horizontal or x component of the injected fuel momentum is the only cause of losses
- Complete momentum mixing is established between stations (1) and (2) i.e., a uniform velocity profile at station (2)

The x components of momentum at station (1) are:

$$\dot{m}_a V_1 + \dot{m}_f V_{fx}$$

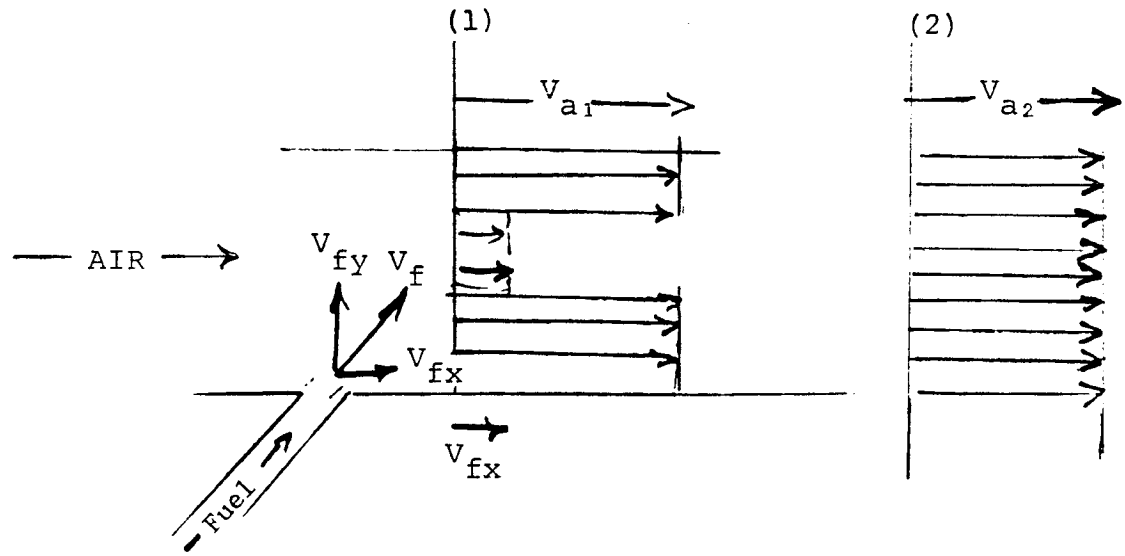

Figure 3.2.1 Fuel Injection Loss Model

Where

$\dot{m}$ = Mass Flow

V = Velocity

Subscript a denotes air

Subscript f denotes fuel

Subscript $_1$ denotes conditions at Station (1)

Subscript $_2$ denotes conditions at Station (2)

Subscript x denotes the x component of flow

Subscript y denotes the y component of flow

The x component of momentum at Station (2) is:

$$(\dot{m}_a + \dot{m}_f)\ V_2$$

Equating the momentum at stations (1) and (2) gives

$$\dot{m}_a\ V_1 + \dot{m}_f\ V_{fx} = (\dot{m}_a + \dot{m}_f)\ V_2 \qquad \text{----------3.2.1}$$

or

$$V_1 + \frac{\dot{m}_f}{\dot{m}_a}\ V_{fx} = \left(1 + \frac{\dot{m}_f}{\dot{m}_a}\right)\ V_2 \qquad \text{----------3.2.2}$$

which can be reduced to

$$V_2 = \frac{\left[1 + \left(\frac{f}{A}\right)\left(\frac{V_{fx}}{V_1}\right)\right]}{\left[1 + \frac{f}{A}\right]} V_1 \qquad \text{----------3.2.3}$$

When $\frac{V_{fx}}{V_1} << 1$ Equation 3.2.3 becomes

$$V_2 \simeq \frac{1}{(1+\frac{f}{a})}\ V_1 \qquad \text{----------3.2.4}$$

or can be written as

$$\Delta V = V_1 \left[\frac{1}{1+\frac{f}{A}} - 1 \right] \qquad \text{----------3.2.5}$$

Utilizing the above assumptions the stagnation pressure ratio between stations (1) and (2) is:

$$\frac{p_{02}}{p_{01}} = \left[\frac{1 + \frac{\gamma-1}{2} M_2^2}{1 + \frac{\gamma-1}{2} M_1^2} \right]^{\frac{\gamma}{\gamma-1}} \qquad \text{----------3.2.6}$$

Further, if the speed of sound between stations (1) and (2) is constant, Equation 3.2.6 can be reduced to

$$\frac{p_{02}}{p_{01}} = \left[1 + \frac{(\gamma-1)\ M_1\ \Delta M_1}{1 + \frac{\gamma-1}{2} M_1^2} \right]^{\frac{\gamma}{\gamma-1}} \qquad \text{----------3.2.7}$$

by setting

$$M_2 = M_1 + \Delta M_1$$

and noting that

$$M_2^2 = M_1^2 + 2M_1\Delta M_1 + \Delta M_1^2$$

and that higher order terms can be neglected.

Further, it is noted from Equation 3.2.4 that

$$M_1 = \left(1 + \frac{f}{A} \right) M_2 \qquad \text{----------3.2.8}$$

and that

$$\Delta M_1 = M_1 \left[\frac{1}{1+\frac{f}{A}} - 1 \right] \qquad \text{----------3.2.9}$$

which substituted into Equation 3.2.7 results in

$$\frac{p_{02}}{p_{01}} = \left[1 - \frac{(\gamma-1)M_1^2 \left(1 - \frac{1}{1+\frac{f}{A}} \right)}{1+\frac{\gamma-1}{2} M_1^2} \right]^{\frac{\gamma}{\gamma-1}} \qquad \text{----------3.2.10}$$

as the equation for approximating fuel injection losses in terms of the stagnation pressure ratio. Equation 3.2.10 provides a good estimate for situations wherein the x component of fuel injection velocities are small relative to the free stream velocities.

For cases where the fuel injection velocity is appreciable Equation 3.2.3 should be used in the derivation to replace Equation 3.2.4 this resulting in

$$\frac{p_{02}}{p_{01}} = \left[1 - \frac{(\gamma-1)\ M_1^2 \left(1 - \frac{1+\frac{V_{fx}}{V_1}\frac{f}{A}}{1+\frac{f}{A}} \right)}{1+\frac{\gamma-1}{2} M_1^2} \right]^{\frac{\gamma}{\gamma-1}} \qquad \text{----------3.2.11}$$

Table 3.2.1 prepared from Equation 3.2.1, presents the fuel injection stagnation pressure ratio losses for mass fuel air ratios of 0.01, 0.03, 0.10, and 0.30. Values for the $\frac{V_{fx}}{V_1}$ ratio were taken from 0 to 1.0 in increments of 0.1.

3.3 Considerations of Fuel Injection and Fuel Injection Losses in Supersonic Airstreams

Efficient fuel injection to supersonic airstream differs from fuel injection to subsonic airstream in several aspects, namely:

- High injection velocities are required and consequently high injection pressures when liquid fuels are utilized
- Large fuel-air ratios induce high losses that can only be ameliorated by downstream injection at velocities approaching those of the free stream
- Losses are dependent upon stoichiometry. The stoichiometric fuel-air ratio for hydrogen is 0.0284 whereas for methane it is 0.0550 or nearly twice that of hydrogen. Methane would, therefore, induce approximately twice the stagnation pressure ratio loss as that of hydrogen. Even distribution of fuel throughout that airstream is difficult to attain without a large number of injection nozzles.

The oblique detonation wave ramjet is expected to possess combustion chamber inlet Mach numbers in the range of 4 to 7 which should result in stagnation pressure ratio losses for stoichiometric fuel-air mixtures of:

Hydrogen -- p_{02}/p_{01} = .83 to .97

Methane -- p_{02}/p_{01} = .70 to .93

Table 3.2.1 Fuel Injection Stagnation Pressure Losses

$\frac{V_{fx}}{V_1}$	M_1	P_{o_2}/P_{o_1}										
		0	.1	.2	.3	.4	.5	.6	.7	.8	.9	1
f/A=.01	2	.970	.973	.976	.979	.982	.985	.988	.991	.994	.997	1.0
	3	.956	.960	.965	.970	.974	.978	.982	.987	.991	.996	1.0
	5	.943	.949	.955	.960	.966	.971	.977	.983	.988	.994	1.0
	7	.939	.945	.951	.957	.963	.969	.975	.981	.987	.994	1.0
	10	.936	.942	.948	.955	.961	.967	.974	.980	.987	.993	1.0
f/A=.03	2	.912	.921	.929	.938	.947	.955	.964	.973	.982	.991	1.0
	3	.875	.887	.899	.911	.924	.936	.949	.961	.974	.987	1.0
	5	.840	.855	.871	.886	.902	.918	.934	.950	.966	.983	1.0
	7	.827	.843	.860	.876	.893	.911	.928	.946	.963	.982	1.0
	10	.819	.836	.853	.871	.888	.906	.924	.943	.962	.981	1.0
f/A=0.1	2	.745	.768	.791	.816	.840	.866	.891	.918	.945	.972	1.0
	3	.647	.678	.709	.741	.775	.810	.846	.883	.921	.960	1.0
	5	.563	.599	.636	.675	.716	.759	.803	.850	.898	.948	1.0
	7	.532	.570	.609	.651	.694	.740	.787	.837	.889	.943	1.0
	10	.514	.553	.593	.636	.681	.728	.778	.830	.884	.941	1.0
f/A=0.3	2	.448	.490	.534	.581	.631	.685	.741	.801	.864	.930	1.0
	3	.292	.337	.387	.443	.504	.570	.643	.722	.807	.900	1.0
	5	.183	.226	.276	.334	.399	.474	.557	.651	.756	.872	1.0
	7	.150	.191	.240	.297	.363	.363	.526	.625	.736	.861	1.0
	10	.132	.172	.219	.276	.342	.420	.508	.610	.725	.854	1.0

4.0 Wave Classification

Classification of one dimensional and oblique waves was discussed in the final report of previous work entitled "The Evaluation of the Oblique Detonation Wave Ramjet" (Contract No. NAS-1-14771). Pertinent portions of the above report follow.

4.1 One Dimensional Wave Classification

One dimensional compressible flow processes can be characterized and usefully classified for the case of normal detonation waves[1] by the introduction of the functions:

$$f \equiv \frac{2(\gamma+1)}{(M_1^2-1)} M_1^2 \left(\frac{Q}{C_p T_1}\right) \qquad \text{----------4.1.1}$$

and

$$F \equiv 1+\sqrt{1-f} \qquad \text{----------4.1.2}$$

into the conservation equations, denoting conditions immediately in front of the normal detonation wave. This results in the following equations for pressure, density, temperature, and downstream Mach number:

$$\frac{p_2}{p_1} = 1 + \frac{F}{\gamma+1} (M_1^2-1) \qquad \text{----------4.1.3}$$

---

[2] Adamson, T.C., and Morrison, R. B., "On the Classification of Normal Detonation Waves, " Jet Propulsion, August 1955

$$\frac{\rho_2}{\rho_1} = \frac{1}{1 - \frac{F}{\gamma+1}\,\frac{M_1^2-1}{M_1^2}} \qquad 4.1.4$$

$$\frac{T_2}{T_1} = \left\{1+\left(\frac{\gamma F}{\gamma+1}\right)(M_1^2-1)\right\}\left\{1-\left(\frac{F}{\gamma+1}\right)\frac{(M_1^2-1)}{M_1^2}\right\} \qquad \text{---------4.1.5}$$

$$M_2 = \sqrt{\frac{(\gamma+1-F)\ (M_1^2-1)+(\gamma+1)}{\gamma F(M_1^2-1)+(\gamma+1)}} \qquad \text{---------4.1.6}$$

Subscript (2) denotes conditions immediately downstream of the normal detonation.

For adiabatic flow, Q = O, and f = 0, making f = 2; i.e., the case of a normal shock wave. For non-adiabatic flows and positive heat addition, $0 < < 1$ defines the range of possible solutions consistent with the one dimensional conservation equations. f = 1 further defines the case of limiting heat addition (thermal choking) and the Chapman-Jouguet (C-J) conditions. Values for f between 0 and 1.0 represent cases of non-limiting heat addition and strong detonations.

4.2 Oblique Wave Classification

The above equation for pressure, density, temperature, and downstream Mach number can be applied to oblique waves if these equations are written in terms of the normal components

to the wave. For a wave angle of β and deflection angle of θ these equations are then:

$$\frac{p_2}{p_1} = 1+ \frac{\gamma F}{\gamma+1} (M_1^2 \sin^2\beta - 1) \qquad \text{----------4.2.1}$$

$$\frac{\rho_2}{\rho_1} = \frac{1}{1- \frac{F}{\gamma+1} \frac{(M_1^2 \sin^2\beta - 1)}{M_1^2 \sin^2\beta}} \qquad \text{----------4.2.2}$$

$$\frac{T_2}{T_1} = \left[1+ \frac{\gamma F}{\gamma+1} (M_1^2 \sin^2\beta - 1) \right] \left[1- \left(\frac{F}{\gamma+1}\right) \frac{(M_1^2 \sin^2\beta - 1)}{M_1^2 \sin^2\beta} \right] \qquad \text{----4.2.3}$$

$$M_2 \sin(\beta-\theta) = \sqrt{\frac{(\gamma-1-F)(M_1^2 \sin^2\beta - 1)+(\gamma+1)}{\gamma F (M_1^2 \sin^2\beta - 1)+(\gamma+1)}} \qquad \text{-------4.2.4}$$

$$\tan\theta = \frac{\frac{F}{\gamma+1} \left(1- \frac{1}{M_1^2 \sin^2\beta}\right) \tan\beta}{1+\tan^2\beta \left[1- \frac{F}{\gamma+1} \left(1- \frac{1}{M_1^2 \sin^2\beta}\right) \right]} \qquad \text{-------4.2.5}$$

The above oblique wave equations are classified in the identical manner of normal waves i.e., F = 2 describes oblique shock waves, F = 1 describes oblique Chapman-Jouguet waves, and 1 < F < 2 strong detonation waves.

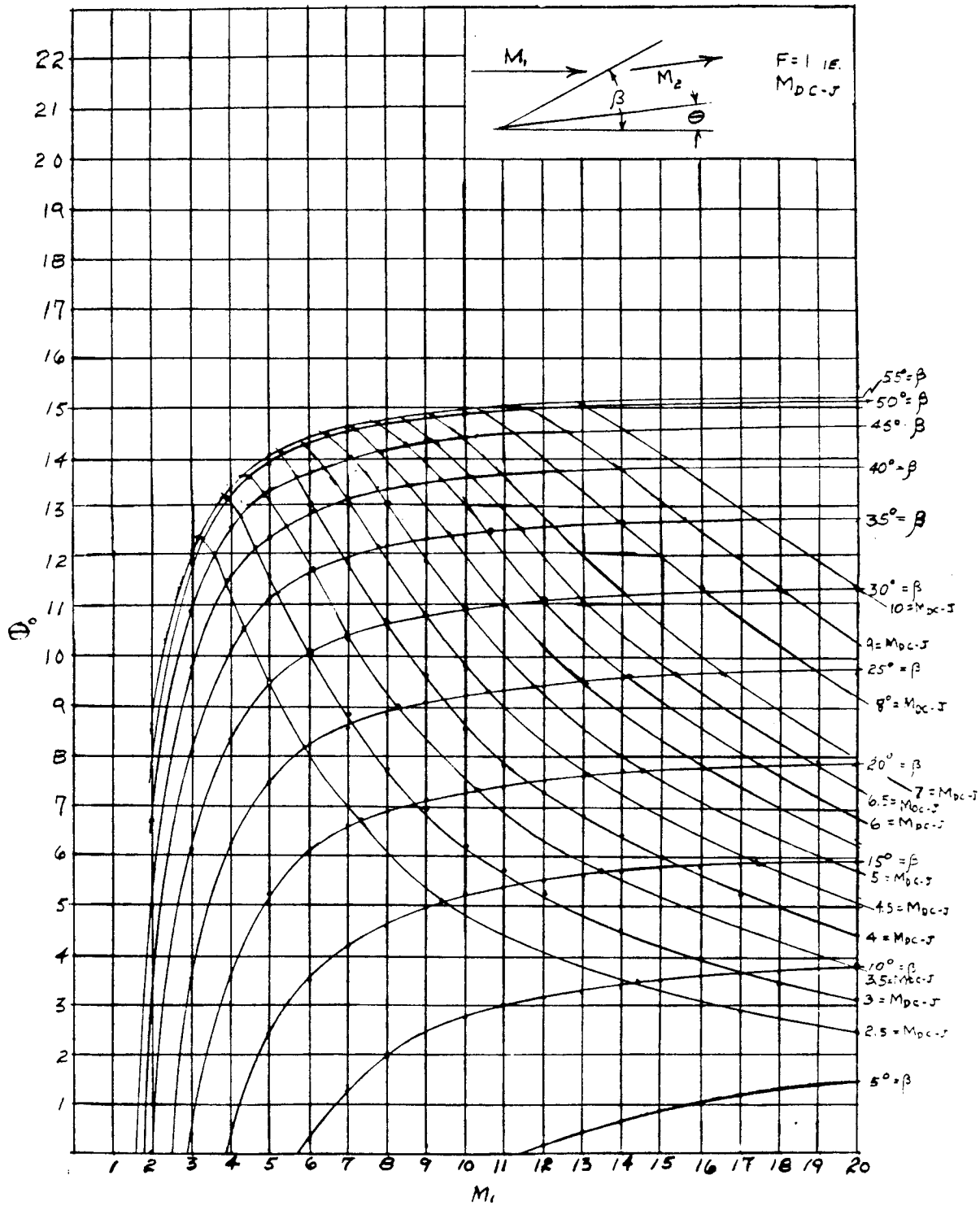

Figure 4.3.1 Oblique Detonation Wave Properties

4.3 Oblique Wave Graphs

The oblique wave equations of Section 4.2 were used to generate a set of tables from which a set of oblique wave graphs could be plotted for a series of F numbers from F = 1 to F = 2.

Figure 2.1.2.1 is the oblique wave graph for F = 2.

Figure 4.3.1 is the oblique wave graph for F = 1.

5.0 Combustion Chamber Configurations

5.1 General

The combustion chamber configuration required is primarily determined by the diffuser design and secondarily by expansion nozzle requirements.

The reflected shock diffuser results in a combustion chamber deep in the internal diffuser duct, which provides long mixing lengths.

The multiple shock diffuser terminates diffusion in the vicinity of the diffuser lip by the intersection of the incident shocks, provides small mixing lengths, and thus requires detonation initiation in the immediate vicinity of the lip to prevent strong shock reflections and over-diffusion of the airstream

Either diffuser configuration requires the use of strong oblique detonation waves if variable geometry is to be avoided under conditions of off-design point operation.

Although strong detonation waves can be rigorously analyzed, the procedures are lengthy and laborious. A practical substitute technique that is simple and sufficiently accurate is offered in the following material of this section.

Figure 5.1.1 is a graph of the defining equations for F where lines for constant heating parameters, $^{Q}/_{C_pT}$, are shown together with the corresponding normal components of the oblique strong detonation waves, which is M_{Dn}. At F = 1,

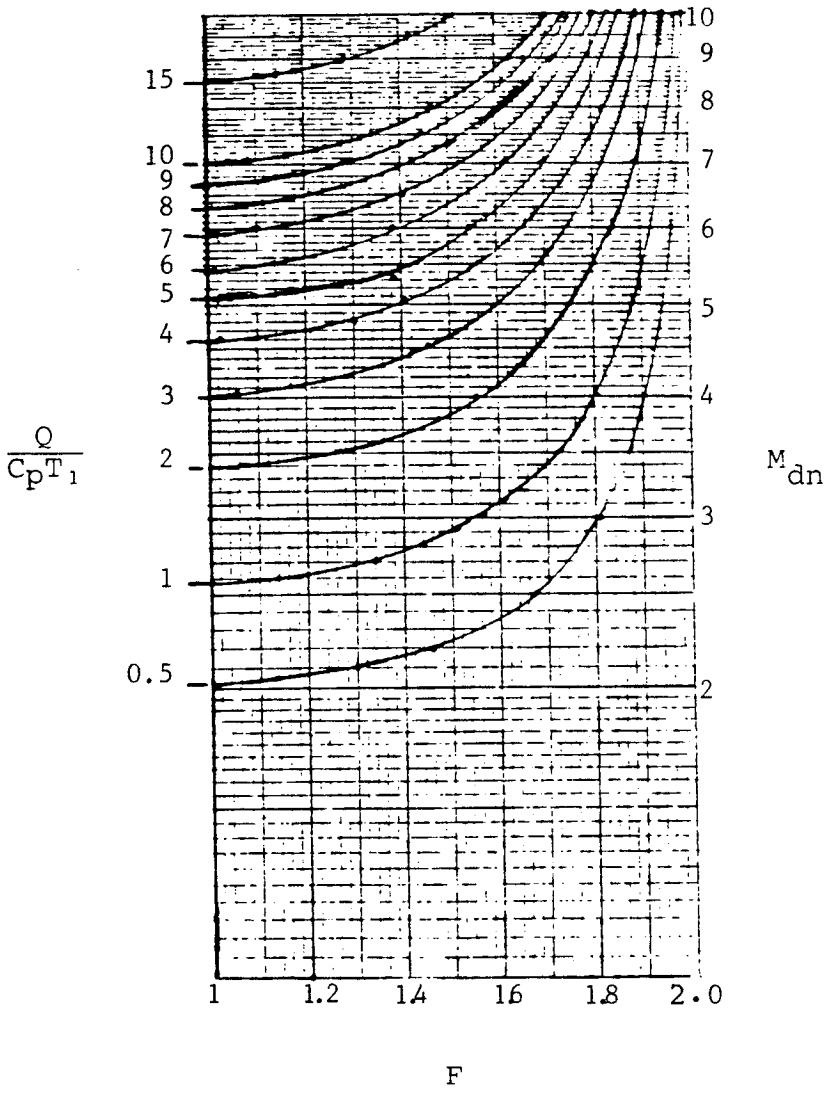

Figure 5.1.1 Heating Parameter versus Wave Classification Number

Q/C_pT, corresponds to $M_{Dn} = M_{DC-J}$, the Chapman-Jouguet Mach number.

Although Figure 5.1.1 is based on perfect gas relations, it can be used with emperical test data for Chapman-Jouguet detonation Mach numbers to establish a real gas point of departure to evaluate strong detonations. For example, in Figure 5.1.1, if measured Chapman-Jouguet detonation Mach number is 6 the corresponding heating parameter is 7.1. Following the 7.1 line to F = 1.6 results in $M_{Dn} = 7.5$.

M_{Dn}, in turn, can be used to determine the gas properties behind the strong oblique detonation wave. Although this technique is non-rigorous it may be used with confidence for small values of F, i.e., 1 to 1.6. At large values of F, i.e., 1.8 to 1.9, serious errors would be incurred, requiring detailed real gas analyses.

5.2 Combustion Chamber for Reflected Shock Diffuser

The configuration of the combustion chamber selected for a 5^0 wedge/ramp reflected shock diffuser is shown in Figure 5.2.1. Reflected Shock Diffuser Combustion Chamber

The fuel injection rake/strut is positioned between stations 14 and 16; a location that allows for two oblique compressions before fuel injection and a two station distance of 14 to 16 as the mixing length to accommodate a range of flight Mach numbers form 4 to 9.

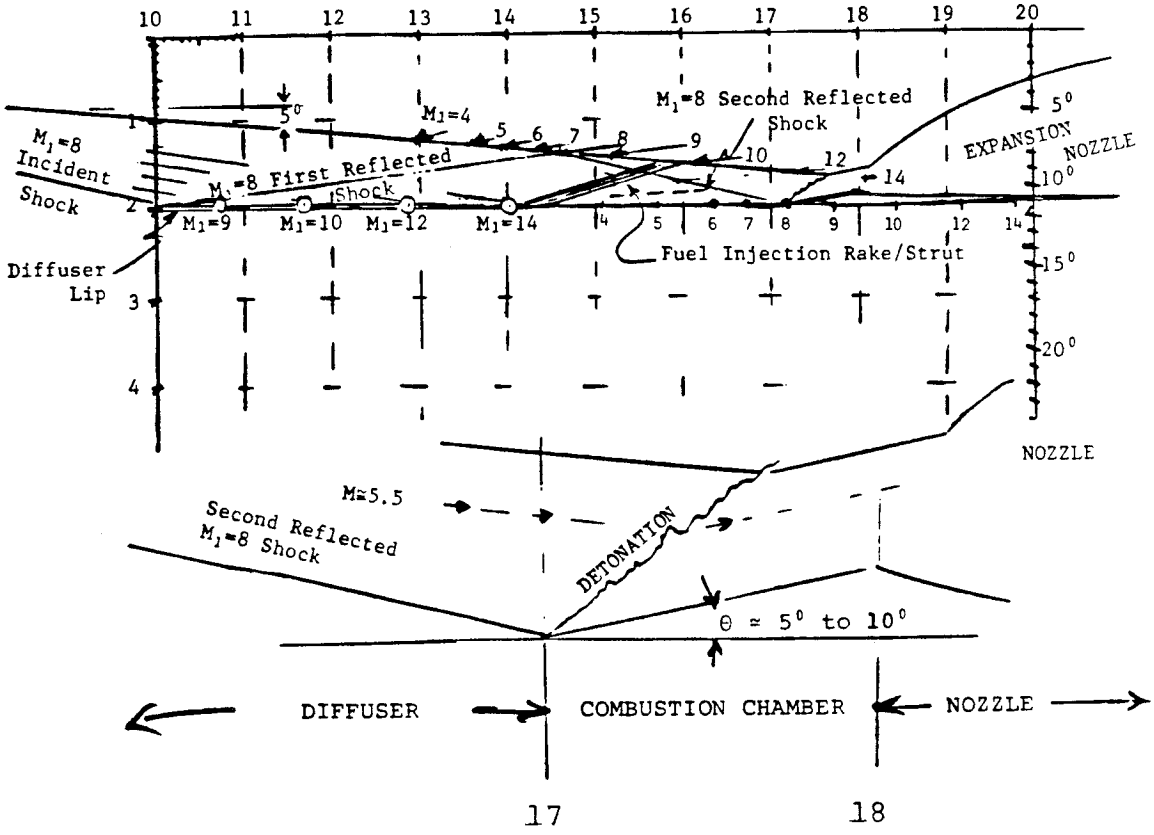

Figure 5.2.1 Oblique Detonation Wave Combustion Chamber for Reflected Shock Diffuser

The combustion chamber, itself, is the zone between stations 17 and 18. The nozzle section is that zone aft of station 18 and the diffuser section that zone forward of station 17.

At design conditions of $M_1 = 8$ the second reflected shock intersects the leading edge of the detonation wedge. The resulting total flow deflection from the wedge plus the second reflected shock is 10^0 to 15^0. Under non-detonating conditions this produces an oblique shock with $M_{1n} \simeq 2.2$

Examination of the temperature behind the $M_{1n} \simeq 2.2$ shock enable one to estimate the ignition delay time. The overall temperature ratio, referred to free stream air temperatures, is approximately 4, or for an inlet temperature of 278^0K, equal to approximately 1200^0K.

From the work of Patch[2] the experimental ignition delay time is in the order of 20 to 50 microseconds for equivalence ratios in the range of 0.125 to 2.75 and at a reduced pressure of 0.148 atmospheres. Inasmuch as higher pressures reduce ignition delays the above may be regarded as a conservative estimate. The latter would produce a delay distance of a few centimeters, i.e., 2 to 4 cm.

---

[1] Patch, Richard W., "Prediction of Composition Limits for Detonation of Hydrogen-Oxygen-Dilutent Mixtures," ARS, 14th Annual Meeting, Washington, D.C. November 16-20, 1959

If the ignition delay time is sufficiently small, detonation will develop with the shock component of the detonation providing temperatures in excess of 3000^0K with corresponding ignition delays under 1 microsecond.

Positive ignition can be promoted by providing a blunt leading edge to the detonation wedge as shown in Figure 5.2.2. A detached shock pattern is produced in advance of the wedge wherein Region (A) exists, behind a normal shock, at approximately free stream stagnation temperatures of 3800^0K with ignition delays in the order of 0.1 microsecond. These conditions are more favorable than those which exist for the stablized oblique detonation wave.

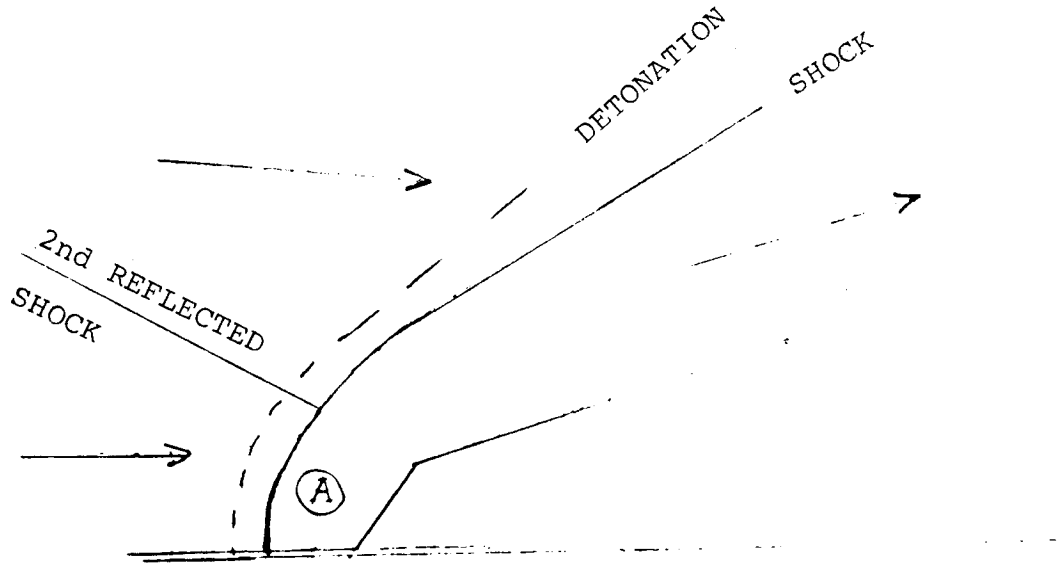

Figure 5.2.2 Detonation Wedge Shock Patterns at $M_1 = M_{design}$

At flight speeds below M_{des} = 8 the second reflected shock moves forward producing the shock pattern shown in Figure 5.2.3. At takeover speed of Mach $M_1 \simeq 6$ the temperature of Region (A) is approximately 2300°K with ignition delay times less than one microsecond.

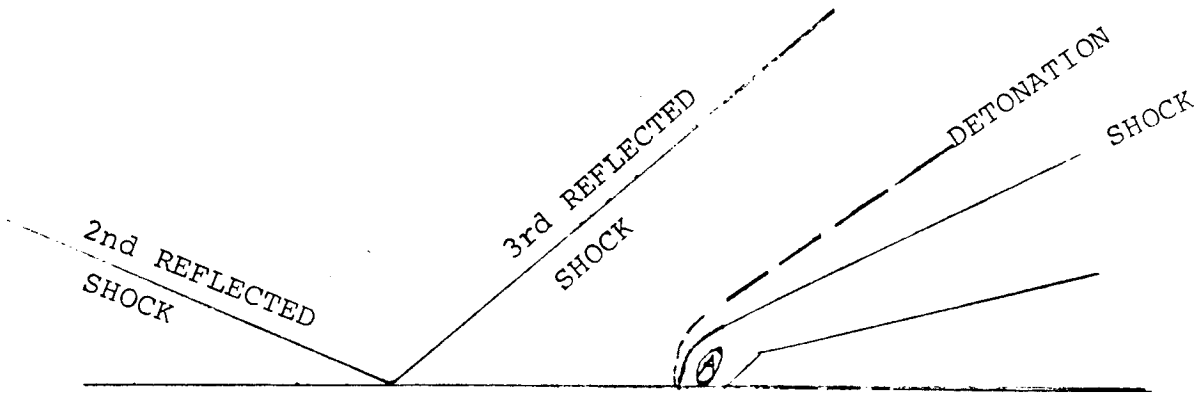

Figure 5.2.3 Detonation Wedge Shock Patterns at $M_1 < M_{design}$

At flight speeds in excess of M_{des} = 8 the second reflected shock moves aft producing the shock pattern shown in Figure 5.2.4. At flight speeds in the order of M_1 = 10 the second reflected shock intersects the detonation wedge in the aft portion of the combustion chamber. Also at M_1 = 10 the first reflected shock intersects the shock wedge at the fuel injection rake/strut. The temperature of Region (A) would ideally approach 5800°K.

At M_1 = 12 the first reflected shock is ingested into the combustion chamber with the second reflected shock passing aft of the detonation wedge into the expansion nozzle.

At M_1 = 14 the first reflected shock is ingested aft of the combustion chamber into the expansion nozzle.

The accommodation of the basic M_{des} = 8 (three shock diffuser) to off-design point operation is to be noted. At flight speeds below design the compression process is more efficient with smaller stagnation pressure ratio losses. This favors lower takeover speeds.

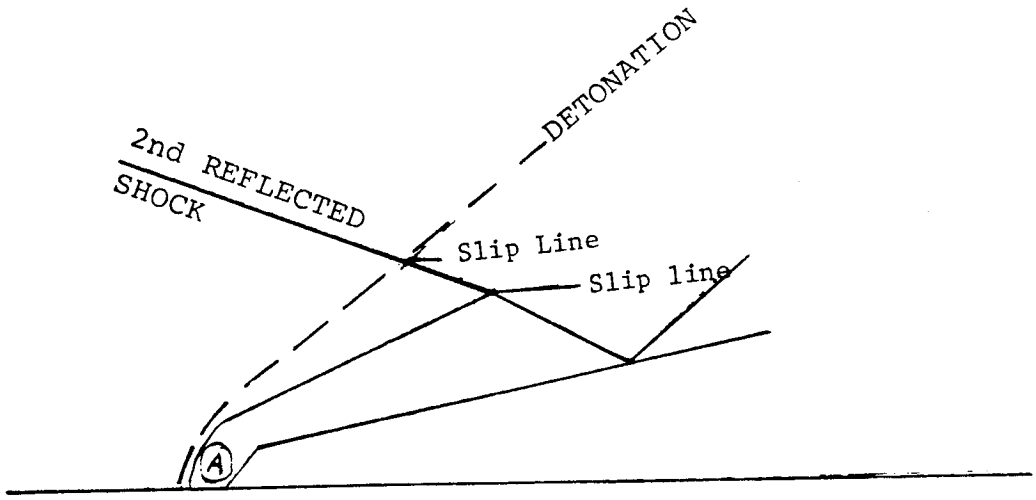

Figure 5.2.4 Detonation Wedge Shock Patterns at $M_1 < M_{design}$

The above, however, is to be balanced with the equivalent stagnation pressure ratio losses associated with spillover.

At flight speeds above design stagnation pressure losses are higher. These losses it should be noted result in much smaller degradations of the thrust coefficients and specific impulses than occur at the lower flight speeds.

Furthermore, at flight speeds above $M_1 \simeq 13$, the ramjet operates as a two shock diffuser and the losses associated with the third reflected shock are dispensed with.

5.3 Combustion Chamber for the Non-Reflected Multiple Shock Diffuser

The configuration of the $M_{des} = 8$ ramjet combustion chamber matching the non-reflected shock diffuser is shown in Figure 5.3.1.

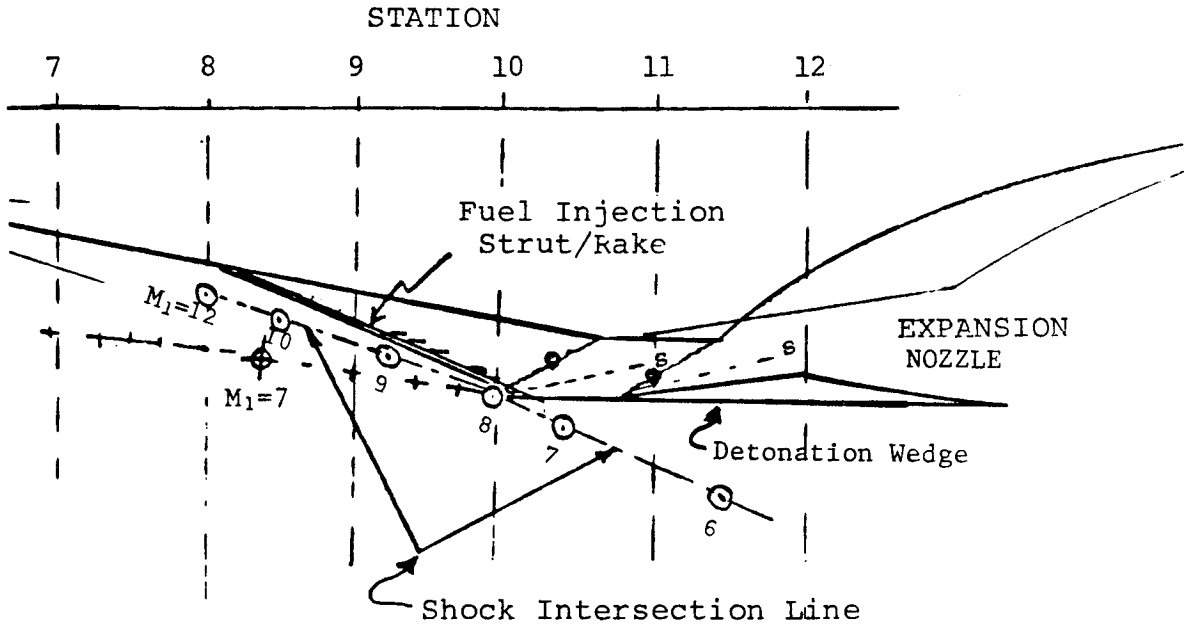

Figure 5.3.1 Combustion Chamber for the $\theta_1 = 5^0$, $\theta_2 = 6^0$ $M_{design} = 8$ Ramjet

The fuel injection rake/strut is located forward of the diffuser lip between station 8 and 10 at a position immediately aft of the incident shock intersection points. This provides for maximum mixing lengths consistent with flight Mach numbers in excess of the design Mach number of 8. A 2-shock compression is provided before fuel injection to accommodate flight Mach numbers from the takeover Mach number. At speeds above the design Mach number the shock configuration shown in Figure 2.3.2 results in a splitting of the compression process; i.e., one 2-shock compression and one 1-shock compression.

The combustion chamber is that zone between stations 10 and 13.

The positioning of a detonation wedge is not critical inasmuch as the diffuser flow has been deflected down 11^0 by the diffuser wedge thereby requiring a very small detonation wedge. At the design Mach number of $M_1 = 8$, for example, and a $M_{DC-J} = 4$, a deflection angle of 12.8^0 is required for establishing an oblique Chapman-Jouguet detonation, i.e., a detonation wedge of 1.8^0. For $M_{DC-J} = 3.3$ an 11^0 deflection results and no detonation wedge is required to establish Chapman-Jouguet conditions.

Figure 5.3.2 details the combustion chamber configuration selected and the positioning of a detonation wedge. Section 5.2 discussed detonability in terms of the temperature

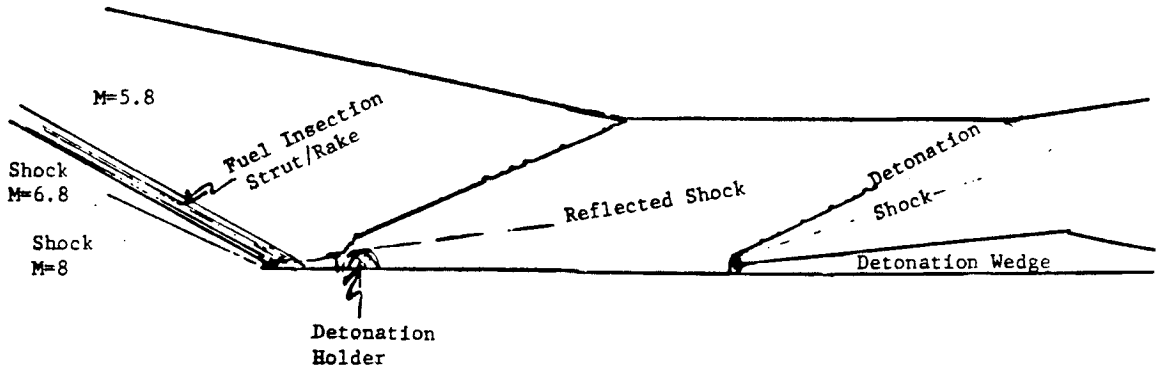

Figure 5.3.2 Combustion Chamber Deatila

conditions in the wake of a shock and a blunt detonation wedge selected to produce the correct flow deflection for an oblique Chapman-Jouguet detonation wave.

The situation described in Figure 5.3.2, which required no detonation wedge for correct flow deflection, does not produce temperatures behind the reflected shock from the diffuser lip sufficient to ensure detonation.

This suggests the use of a blunt small angle detonation wedge to force strong detonations. The wedge detonation holder could be positioned fore and aft along the diffuser lip to satisfy off-design point operations. At low flight Mach numbers a forward position is desired, with high flight Mach numbers requiring an aft position.

The lack of accommodation this multiple shock diffuser provides to off-design operation of the combustor is noted. Excessive spillover exists for low flight speeds and large stagnation pressure ratio losses at high speeds.

6.0 Chemical Effects Upon the Oblique Detonation Wave Ramjet

6.1 Detonation Limits and Ignition Time Delay

Figure 6.1.1 is a graph of experimental ignition time delays versus temperature taken from Patch's[3] work wherein the experimental data from several investigators were correlated.

The portion of the graph from 1100°K to 3000°K represents the experimental work of Schott and Kinsey[4] for hydrogen-oxygen-argon mixtures at a reduced pressure of 0.148 atmospheres.

Patch reports that the knee of the curve in Figure 6.1.1 occurs at approximately 1100°K whereas a temperature of 1314°K was the calculated value of ignition temperature after shock for mixtures at the theoretical detonation limit. This discrepancy is attributed to the use of these theoretical detonation velocities.

The dashed curve below the main curve represents an estimated ignition delay time correction of the 0.148 atmosphere data to 1 atmosphere pressure.[5]

As a criterion for application to the oblique detonation wave ramjet the following assumptions are made for the use of Figure 6.1.1:

---

3 Ibid

4 Schott, G. L. & Kinsey, J. L., Kinetic Studies of Hydroxyl Radicals in Shock Waves. II. Induction Times in the Hydrogen-Oxygen Reaction, J. Chem. Phys., Vol. 29, No. 5, Nov. 1958, pp 1177-1182.

5 Huber, P. W., Schexnayder, D. J. Jr., & McClinton, C. R., Criteria for Self-Ignition of Supersonic Hydrogen-Air Mixtures, NASA Technical Paper 1457, Aug. 1979, p 36.

- Shock compressions that result in static temperatures under 900°K to 1000°K possess sufficiently long ignition delay times that combustion will not take place prior to detonation in the ramjet combustor

- Detonation is initiated when conditions behind the initiating shock possess a static temperature in excess of 2000°K.

The previous report, "Evaluation of the Oblique Detonation Wave Ramjet," emperically established a temperature detonation limit of 1000°K upon the required multi-shock diffuser performnace. Figure 6.1.2 taken from the above report, is validated in terms of data presented in Figure 6.1.1.

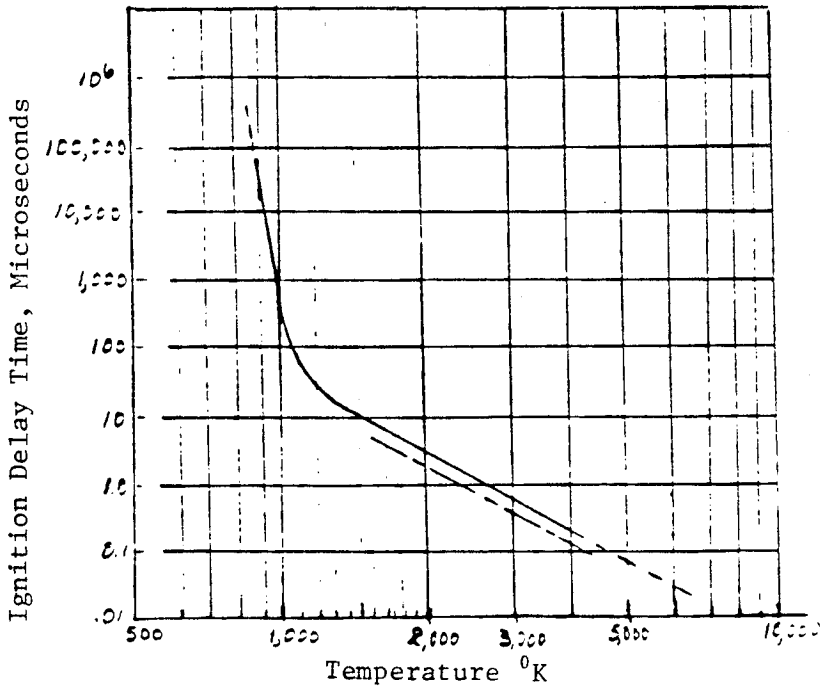

Figure 6.1.1 Ignition Delay Times

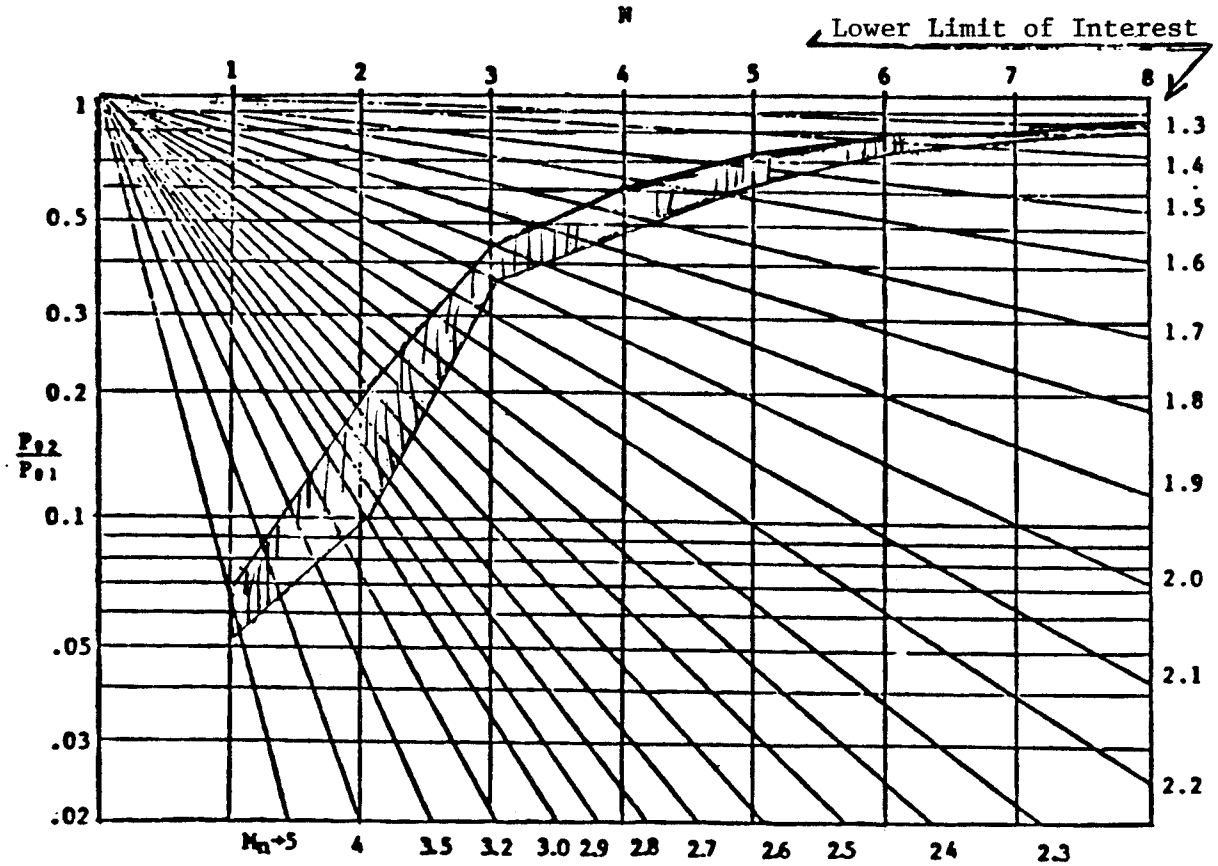

Figure 6.1.2 Effect of Temperature Detonation Limit Upon Required Multi-Shock Performance

6.2 Dissociation Effects

The properties of the ideal hydrogen-air reaction going to completion is shown in Figure 6.2.1.

$H_2 + \frac{1}{2} O_2 + 1.86\ N_2 \rightarrow H_2O + 1.86\ N_2 + 51{,}571$ cal./gm.

	H_2	O_2	N_2	H_2O	N_2
gm. Mol. wgt.———	2	16	52.1	18	52.1
Percent by Wgt.———————	2.85	22.8	74.3	25.7	74.3
Volume Percent	29.8	14.9	55.4	35	65

Figure 6.2.1 Ideal Hydrogen-Air Reaction

For stoichiometric mixtures of H_2 and air at atmosphere pressure, and an initial temperature of 298^0K, combustion produces a theoretical flame temperature of 2350^0K with the gas composition shown in Figure 6.2.2.

gas	N_2	O_2	H_2	NO	H_2O	H	O	OH
Volume %	62.8	.5	1.8	.3	33.8	.19	.06	.65

Figure 6.2.2 Theoretical Equilibrium Composition of the Combustion Products of a Stoichiometric Mixture of Hydrogen-Air

Clearly the difference in composition as compared to ideal reaction is small with 6 volume percent of the H_2 and 3 volume percent of the O_2 unreacted. The formation of 0.3 volume percent of NO is the only side reaction which would influence the basic gas phase reactions of pure hydrogen-oxygen mixture. Also all these dissociation effects are maximum at near stoichiometric conditions.

Without incurring significant error it can be assumed that the NO reaction may be neglected and the dominant basic gas phase reactions are:

$$H_2O \rightleftharpoons H_2 + O$$

$$H_2O \rightleftharpoons \tfrac{1}{2} H_2 + OH$$

$$H_2 \rightleftharpoons 2H$$

$$O_2 \rightleftharpoons 2O$$

Further, noting from Figure 6.2.2 that the percent of monatomic H and O are also small, it may be assumed that the dissociation of H_2O into H_2 and O_2 is the dominant reaction for evaluation purposes.

The equilibrium constant for the reaction $H_2 + \tfrac{1}{2}O_2 \rightleftharpoons H_2O$ at 2500^0K[5] is:

$$K_p = \frac{P_{H_2} P_{O_2}}{P_{H_2O}} = 6 \times 10^{-3}$$

---

5 Morrison, R. B. and Ingle, M. J., Design Data for Aeronautics and Astronautics, University of Michigan, John Wiley & Sons, Inc., 1961, p 464.

where the partial pressures p_{H_2}, p_{O_2}, and p_{H_2O}, are the partial pressures in atmospheres. For the combustion of stoichiometric hydrogen-oxygen mixture at 1 atmosphere the calculated compositions are shown in Figure 6.2.3 where these are compared to those taken from NACA Report 1383.

	H_2	O_2	H_2O
NACA Report 1383	.05	.014	.936
Approximation Technique	.029	.0145	.957

Figure 6.2.3 Composition of Gases for the H_2-O_2 Reaction

The discrepancies between the approximation values and those of the NACA Report 1383 can be attributed largely to the formation of monatomic hydrogen and monatomic oxygen. The formation of a small amount of NO would account for most of the residual discrepancies.

It is concluded that the dissociation effects associated with the combustion hydrogen-air mixtures are minimal; amounting to a maximum of a few percent (4% to 6%) of dissociated water under stoichiometric conditions. Lean mixtures would possess insignificant dissociation.

Combustion of hydrocarbon-air mixtures, unlike the combustion of hydrogen-air mixtures, is influenced to a large extent by carbon reactions with oxygen; i.e., carbon combining with oxygen at the expense of hydrogen combining

with oxygen. The reaction of a 50 percent mixture of acetylene and oxygen is a good example. The course of this reaction has been shown to be:

$$C_2H_2 + O_2 \rightarrow 2CO + H_2$$

The reaction of methane with oxygen is another example, the combustion of rich mixtures of methane being one method of producing hydrogen.

The influence of the above effects upon the detonation process is quite different from that of the deflagration process. Detonation approximates a constant volume process whereas deflagration approximates a constant pressure process. The effects of this difference of processes become marked when applied to the highly dynamic situation of combustion in supersonic flows. Deflagration rates are governed by leisurely multiple diffusion processes whereas detonation rates are determined by exceedingly rapid "compression" processes.

Detonation speeds or velocities are largely dependent upon the heat release, however, they also depend upon the molecular weight change across the detonation front. A decrease in molecular weight across the front enhances the detonation process by increasing the pressure and wave velocity.

Dissociation of combustion products which decrease gas molecular weights, compensates for the heat release

losses associated with dissociation.

The equations for detonation Mach number functionally relate the dependence, i.e.:

$$\text{(Empirical)} \quad M_D = 2.37\ \phi^{\frac{1}{3.05}} \qquad \text{----------6.1}$$

$$\text{(Theoretical)} \quad M_D = 1.54\ \phi^{\frac{1}{2}} \qquad \text{----------6.2}$$

$$\phi = \frac{m_1}{m_2}\frac{Q}{C_p T_1} \qquad \text{----------6.3}$$

Where:

M_D = Mach number of detonation

m_1 = Molecular weight of gases before detonation

m_2 = Molecular weight of gases behind detonation

Q = Heat release

$C_p T_1$ = Gas enthalpy of gases before detonation

ϕ = As defined above, Equation 6.3

Figure 6.2.4, for the detonation velocities of several hydrocarbon-oxygen mixtures, illustrates, graphically the dominance that the molecular weight change exerts over that of heat release. Considering only the heat release, the curves would peak at stoichiometric mixture ratios. No peak is indicated, however, for any of the hydrocarbons. The hexane curve even exhibits a reflex at near stoichiometric mixture ratios, indicating that all the more complex hydrocarbons can be easily detonated.

The detonation of hydrogen and oxygen results in a

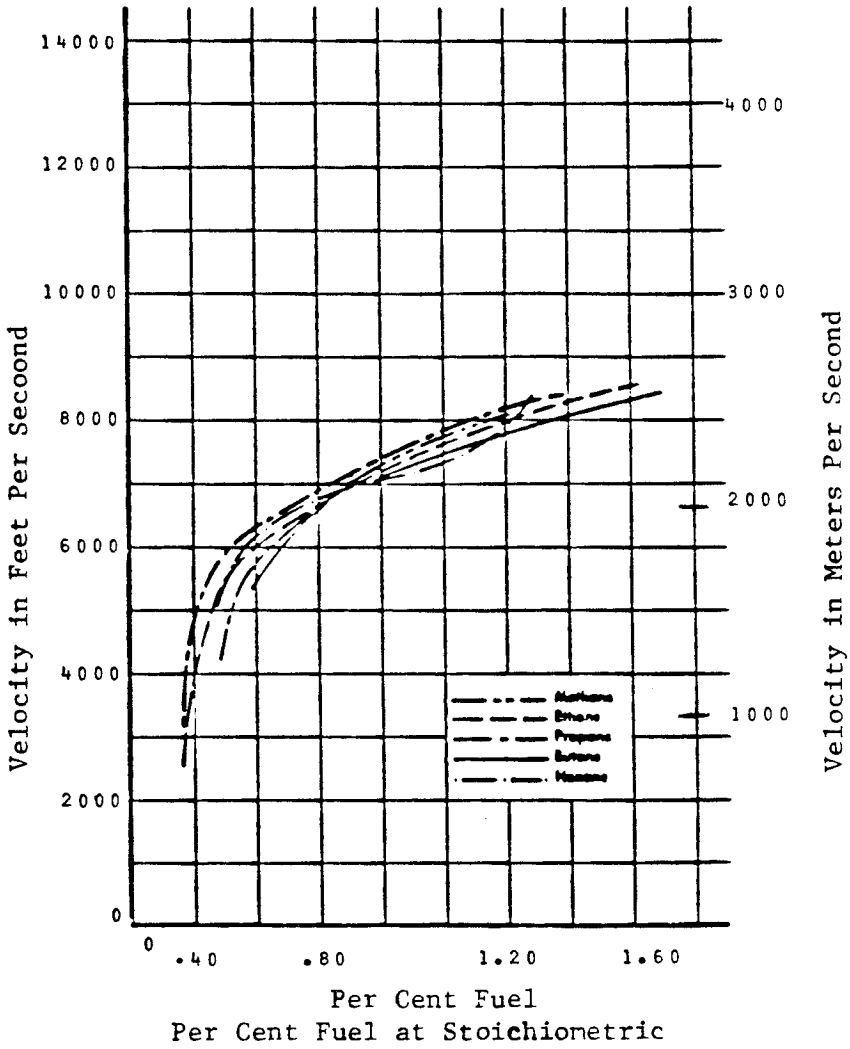

Figure 6.2.4 Detonation Velocity of Gaseous Hydrocarbon-Oxygen Mixtures versus Normalized Mixture Ratio

molecular weight increase across the front. Specifically, considering the reaction:

$$2H_2 + O_2 \rightarrow 2H_2O$$

the molecular weight change across the front, m_1/m_2 is $2/3$. Although the hydrogen-oxygen reaction is one of the most energetic chemical reactions known, and its application to constant pressure processes is very effective; its application to constant volume processes, such as detonation, results in some degradation of performance of the oblique detonation wave ramjet because of this molecular weight increase.

7.0 Expansion Nozzle

7.1 General Considerations

The design of the expansion nozzle for the oblique detonation wave ramjet differs from that of the classical one-dimensional axial flow rocket nozzle in two respects, i.e., asymmetric location of the diffuser nozzle walls, and the absence of a sonic throat. (See Figure 7.1.1)

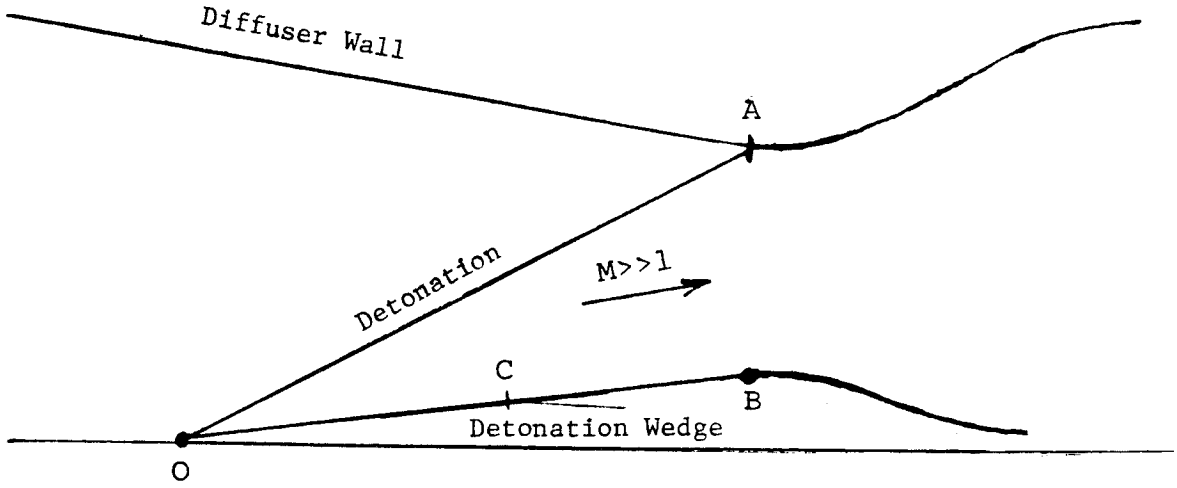

Figure 7.1.1 Oblique Detonation Wave Ramjet Nozzle

Several possible techniques can be employed which depend upon the performance characteristics desired, the geometric complexities to be tolerated, and the strength of the oblique detonation wave employed. Three of these possibilities are:

- Continue detonation wedge back to the point opposite to the point of collision of detonation wave with the diffuser wall, point A in Figure 7.1.1, with section A-B becoming the minimum area section. Thereafter standard nozzle techniques can be used.

- Use of a detonation holder/bump at point O, with no detonation wedge. This results in an oblique Chapman-Jouguet detonation wave immediately followed by a centered rare-faction wave.

- Continue detonation wedge a short distance back to a point, such as C in Figure 7.1.1, and initiate asymmetric expansion of nozzle gases from point C and A.

From the minimum area section aft, the nozzle standard area ratio tables or graphs can be used to establish the desired nozzle contours.

7.2 Nozzle Gas Properties

The products of combustion from the detonation of stoichiometric hydrogen-air mixtures are mostly molecular nitrogen and water. A small mount of water will dissociate (3-5 volume percent) into molecular hydrogen and oxygen and a neglible amount of molecular nitrogen reacts with oxygen to form NO (0.3 volume percent). Section 6 of this report discusses the above in more detail.

Molecular nitrogen properties dominate the expansion process as modified by the presence of water vapor.

The specific heat ratio, $\gamma = {}^{C_p}/_{C_v}$, is shown in Figure 7.2.1 for nitrogen through a temperature range of 100^0K to 3000^0K. For the range of temperatures of 1500^0K to 2500^0K that are encountered in the post-detonation expansion process an average γ of 1.3 is appropriate. It is further noted the γ is insensitive to pressure at these temperatures.

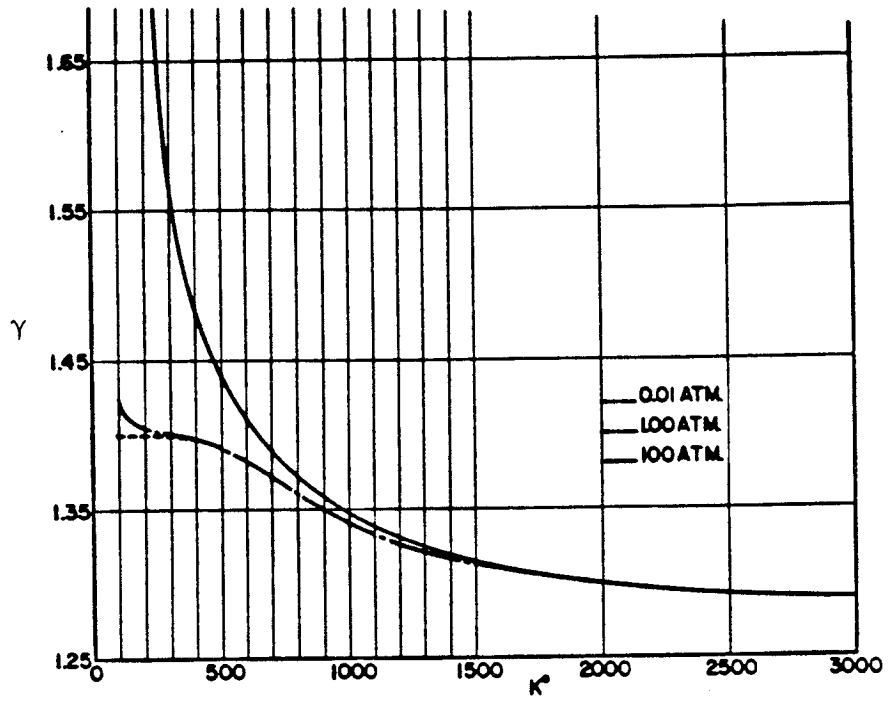

$$\gamma = \frac{C_p}{C_v}$$

Figure 7.2.1 Specific Heat Ratio of Nitrogen

Little specific heat data exists for water vapor at temperature above 1000°K. Extrapolation of specific heat data from 850°K to 2000°K results in a $\gamma = 1.25$. Like molecular nitrogen, the γ for water is insensitive to pressure at these high temperatures associated with the detonation process.

7.3 Expansion Nozzle Properties for $\gamma = 1.3$

The expansion nozzle properties for $\gamma = 1.3$ are shown in Table 7.3.1.

M	A/A*	T_o/T	P_o/p	M	A/A*	P_o/p	T_o/T
1	1	1.15	1.832	4.5	27.28	423.1	4.04
1.5	1.189	1.34	3.526	5.0	45.95	855.7	4.75
2.0	1.773	1.60	7.665	6.0	120.1	3115	6.40
2.5	2.954	1.94	17.56	7.0	285.3	9862	8.35
3.0	5.159	2.35	40.55	8.0	623.0	2.77×10^4	10.60
3.5	9.108	2.84	91.77	9.0	1265	$7.06 \times^4$	13.15
4.0	15.94	3.40	200.9	10.0	2415	1.65×10^5	16.00

Figure 7.3.1 Nozzle Properties for $\gamma = 1.3$

These area ratios and stagnation pressure ratios are for the isentropic expansion of a gas possessing a ratio of specific heats of

Values were calculated from the isentropic flow equations:

$$\frac{A}{A^*} = \left(\frac{1}{M}\right) \frac{\left[1 + \frac{\gamma-1}{2} M^2\right]^{\frac{\gamma+1}{2(\gamma-1)}}}{\left[\frac{\gamma+1}{2}\right]^{\frac{\gamma+1}{2(\gamma-1)}}} \qquad \text{----------(7.3.1)}$$

$$\frac{p_o}{p} = \left[1 + \frac{\gamma-1}{2} M^2\right]^{\frac{\gamma}{\gamma-1}} \qquad \text{----------(7.3.2)}$$

$$\frac{T_o}{T} = 1 + \frac{\gamma-1}{2} M^2 \qquad \text{----------(7.3.3)}$$

8.0 Oblique Detonation Wave Ramjet Configurations and Performance

8.1 General Considerations

Section Two discusses the various diffuser configurations and the advantages/disadvantages of each. For a design Mach number of 8, two diffuser types emerged as suitable for a fixed geometry ramjet, i.e.:

- A two-shock multi-shock diffuser with deflection angles of $\theta_1 = 5^0$ and $\theta_1 = 6^0$
- A reflected shock diffuser with a ramp angle of $\theta = 5^0$

The multi-shock diffuser offers the most compact and efficient results at the design point, however, it suffers performance degradations for off-design point conditions.

The reflected shock diffuser, while not as compact as the multi-shock diffuser, is nearly as efficient at the design point and provides good performance for a range of flight Mach numbers.

Sections 3, 5 and 7 discuss fuel injection rates, combustion chamber configurations, and expansion nozzles

8.2 Two-Shock Multi-Shock Diffuser Oblique Detonation Wave Ramjet Configuration

The configuration of the multi-shock oblique detonation wave ramjet is shown in Figure 8.2.1 (page 71). Inherent to this configuration is the difficulty of providing an adequate

mixing length for the injected fuel. In order to alleviate this condition several compromises are made; namely:

1) The fuel injection strut is raked forward from the diffuser lip at an angle approximately equal to and somewhat less than the angle of the shock intersection line.

2) A constant area mixing length is provided between Stations (10) and (11) to allow mixing of that fuel which is injected near the diffuser lip.

3) A detonation wedge is provided at Station (11) to ensure detonation of the fuel-air mixture. A detonation wedge is not required if detonation is attained at Station (10) at the diffuser lip.

The expansion nozzle is arbitrarily shown in Figure 8.2.1 to possess an exit area equal to the frontal intercept area

There are several non-redeeming features of this multi-shock configuration that seriously limit its performance to a region near design point conditions.

At low flight Mach numbers the incident shocks intersect below and behind the diffuser lip. This results in large spillage losses, which in turn increase the Mach numbers at which takeover can occur.

At high flight Mach numbers the incident shocks intersect above and in front of the diffuser lip. This leads to the formation of a third shock possessing high losses, that intersects the diffuser wall behind the diffuser lip.

Also at high flight Mach numbers the lower portion of the fuel injection strut near the diffuser lip is exposed to freestream conditions that lead to high losses for the fuel injection systems.

The multi-shock oblique detonation wave ramjet represents a configuration producing high performance at design point conditions but whose performance is degraded when the latter conditions are not met.

8.3 Reflected Shock Diffuser Oblique Detonation Wave Ramjet Configuration

The configuration of the reflected shock oblique detonation wave ramjet is shown in Figure 8.3.1, (page 72).

Although this design is not compact, it represents an extremely simple geometric configuration possessing excellent performance characteristics through a wide range of off-design point conditions.

Several features of this configuration which result in its excellent performance characteristics are:

- Minimized spillover at low flight Mach numbers is favorable to low takeover speeds
- The location of the fuel injection strut provides adequate mixing lengths in the wake of a two-shock compression for a wide range of flight Mach numbers
- Unlike the multi-shock ramjet (Section 8.2), wherein incident shock intersections result in high loss third shocks, the reflected shock ramjet always reflects a lower loss oblique shock.

- The collapsing and expanding nature of the reflected shock waves, accordion style, that occurs for flight Mach numbers below and above that of design is a compensating factor for the compression process. At $M_1 = 5$, for example, a four shock compression process is realized, whereas at $M_1 = 12$ a two-shock compression process results.

The reflected shock oblique detonation wave ramjet represents a very simple geometric shape with a wide latitude of off-design point capabilities.

8.4 Performance of the Two-Shock Multi-Shock Diffuser Oblique Detonation Wave Ramjet Configuration

Section 8.2 qualitatively discusses the general characteristics of the multi-shock oblique detonation wave ramjet.

Table 8.4.1 (page 75) presents the performance of this configuration in terms of the thrust coefficients and specific impulses for flight Mach numbers of 6, 8 and 10. The design Mach number is 8. Thrust coefficients in Table 8.4.1 are as defined by Equation 2.1.1.1.

The contribution to stagnation pressure losses of the ramjet components are also shown in Table 8.4.1. It is noted that the largest stagnation pressure losses occur for the detonation wave. The shock portion of the detonation wave, however, is the largest portion of this loss.

For example, from Table 8.4.1, with $M_1 = 8$ and $\phi = {}^{2}/_{3}$, a value of 0.0588 is obtained for the stagnation pressure ratio across the detonation. The shock portion of the detonation accounts for a stagnation pressure ratio of approximately 0.1.

Ideally, for a multi-shock diffuser match to the oblique detonation wave, the strength of the oblique shocks should be equal and, also, equal to the strength of the oblique shock portion of the detonation wave. This would suggest the use of larger deflection angles in the diffuser design. To do so, nevertheless, results in a narrowing of off-design point limits. In table 8.4.1, for example, at $M_1 = 6$ and $\phi = 1$, NA designates the detachment of the detonation wave and an operational point that cannot be attained. This constitutes one limit on the ramjet takeover speed.

Also the increasing of deflection angles narrows the limits for high speed flight; this caused from larger diffuser losses.

Figure 8.4.1 (page 75) is a graph of the thrust coefficient flight Mach nubmers of 6 through 10 for equivalence ratios of $\phi = {}^1/_3$, $\phi = {}^2/_3$ and $\phi = 1$. The thrust coefficient, C_T, has been corrected for fuel flow i.e., the equivalence ratio, ϕ, for hydrogen-air mixtures.

8.5 Performance of the Reflected Shock Diffuser Oblique Detonation Wave Ramjet Configuration

Section 8.3 qualitatively discusses the general characteristics of the reflected shock oblique detonation wave ramjet.

The performance of this configuration is shown in Table 8.5.1 (page 77). Also the stagnation pressure ratio-losses

of the various ramjet components are included in that Table.

It is noted that the oblique detonation wave is detached at $M_1 = 6$ and $\phi = 1$. A takeover speed at $M_1 = 6$ could be accomplished for $\phi = {}^2/_3$.

Figure 8.5.1 (page 76) is a graph of the thrust coefficient versus flight Mach number for $\phi = {}^1/_3$, ${}^2/_3$, and 1. It is noted that the performance of the reflected shock ramjet always exceeds that of the multiple shock ramjet except in the region of the design point at $M_1 = 8$ and $\phi = 1$.

8.6 Comparison of the Diffusive Burning Scramjet with the Oblique Detonation Wave Ramjet

The comparison of the hydrogen-fueled detonation ramjet with the hydrogen-fueled scramjet is made on the basis of thrust coefficients as defined by Equation 2.1.1.1.

The scramjet information includes losses encountered from fuel injection, diffusive burning, and nozzle expansion. Calculation of the scramjet thrust coefficients were made from S. Z. Pinckney's work as reported in NASA TM X-74038, 1977, and are, therefore, based upon installed performance.

The thrust coefficients for the detonation ramjet were calculated for the reflected shock configuration. (See Table 8.5.1 and Figure 8.5.1)

The above calculations include the following losses or conditions:

- Diffuser shock losses are evaluated in terms of the stagnation pressure losses. Spillover losses at low flight Mach numbers are accounted for.
- Skin-friction losses and shock-boundary layer interaction effects are not considered.
- Fuel injection losses are evaluated for the high loss case of lateral injection of the hydrogen fuel.
- Fuel injection strut drag/losses are not included
- Detonative combustion losses include the real gas effects obtained from experimental hydrogen-air detonation properties.
- The effects of dissociation are discussed in section 6.2. It is concluded that the dissociation effects associated with the combustion of hydrogen-air mixtures are minimal, amounting to a maximum of 4 percent to 6 percent of dissociated water for stoichiometric conditions.
- Lean mixtures would possess insignificant dissociation. Frozen equilibrium of the expansion gases is assumed.
- Nozzle expansion losses are neglected on the basis that expansion to atmospheric pressure is permitted by the vehicle configuration.

Figure 8.6.1 (page 77) shows the thrust coefficient comparison. The diffusive burning ramjet operating with $\phi = 1$ is to be compared to the detonation ramjet operating with $\phi = 1$.

The oblique detonation wave ramjet compares very favorably with the diffusive burning ramjet at flight Mach numbers of 7 to 8. Its takeover speed, however, occurs at $M_1 \cong 7$, whereas the takeover speed of the diffusive burning scramjet is in the region of $M_1 \cong 4$.

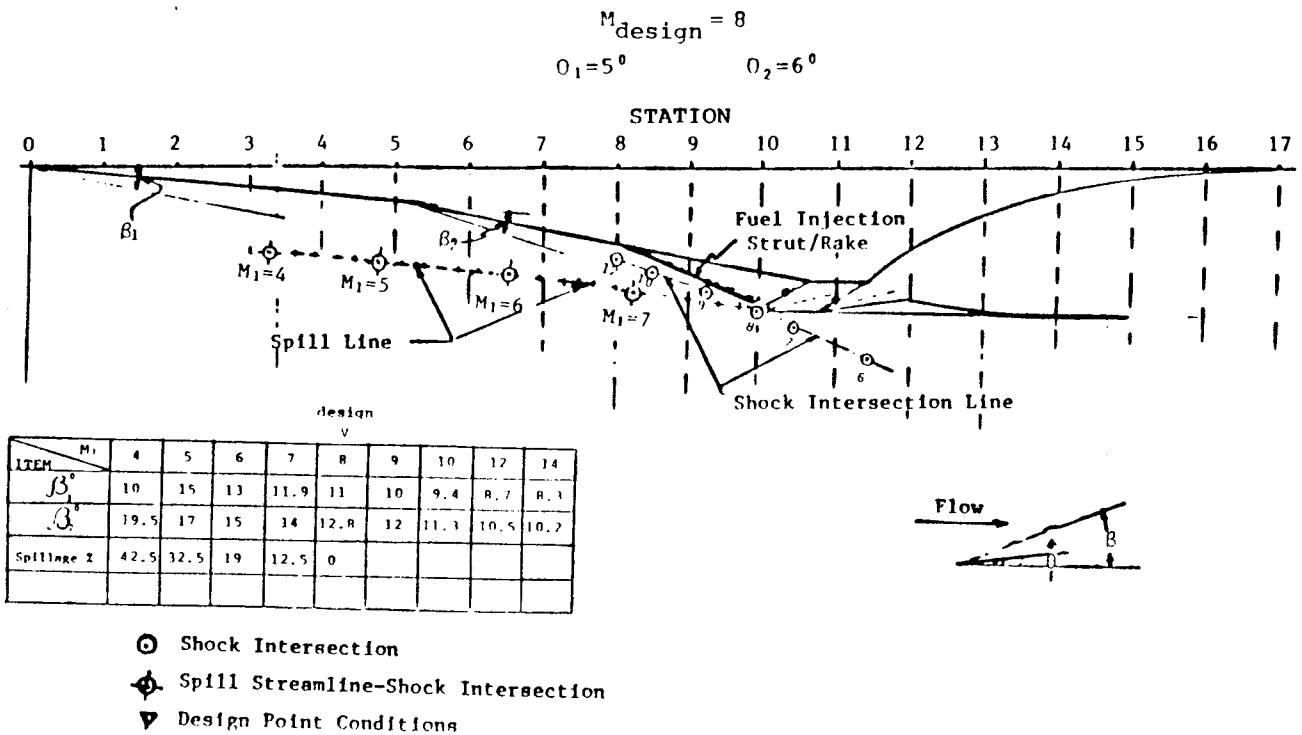

design

ITEM \ M_1	4	5	6	7	8	9	10	12	14
β_1^0	10	15	13	11.9	11	10	9.4	8.7	8.3
β_2^0	19.5	17	15	14	12.8	12	11.3	10.5	10.2
Spillage %	42.5	32.5	19	12.5	0				

Figure 8.2.1 Two-Shock Multi-Shock Diffuser
Oblique Detonation Wave Ramjet

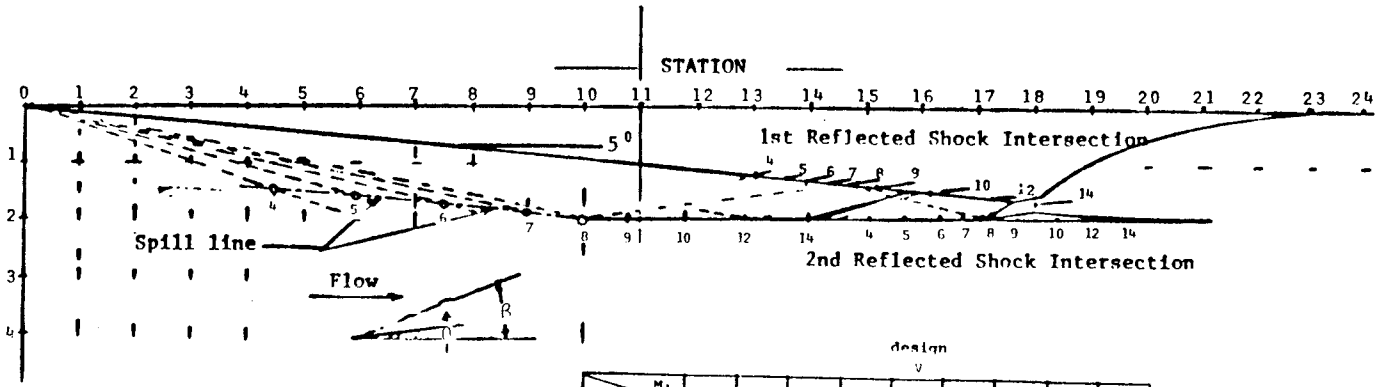

design
M_1

ITEM	4	5	6	7	8	9	10	12	14
β_1°	18	15	13	11.9	11	10	9.4	8.7	8.2
β_2°	19	15.5	14.2	13	12	11.5	10.7	9.7	9
β_1°	19.5	18	15	14.5	13.5	12.5	11.9	11	10.2
Spillage %	25.7	19	12.9	5.1	0	0	0	0	0

Figure 8.3.1 Reflected Shock Diffuser Oblique Detonation Wave Ramjet Configuration

Table 8.4.1 Performance of the Two-Shock $\Theta_1 = 5^0$, $\Theta_2 = 6^0$ Oblique Detonation Wave Hydrogen-Air Ramjet

	M=6			M=8			M=10			
	19% Diffuser Spill						27.5% Flow Through Third Shock			
	$\phi=1/3$	$\phi=2/3$	$\phi=1$	$\phi=1/3$	$\phi=2/3$	$\phi=1$	$\phi=1/3$	$\phi=2/3$	$\phi=1$	Remarks
C_T Ideal	.23	.40	.59	.14	.26	.38	.09	.18	.26	Uncorrected for f/A
C_T Uncorrected f/A	.1215	.235	NA	.095	.19	.285	.0456	.129	.187	Corrected for Spill + M_1=6
C_T Corrected f/A	.132	.258	NA	.105	.213	.322	.0555	.150	.221	
I_{sp} Ideal	4700	4400	4100	3900	3700	3500	3300	3150	3000	
I_{sp} Uncorrected	2511	2430	NA	2600	2750	2700	1630	2260	2290	
I Corrected f/A	2728	2668	NA	2874	3083	3050	1984	2628	2706	
Diffuser-Shock Stagnation Pressure Ratio	.932	.932	.932	.855	.855	.855	.764 / .3797	.764 / .3797	.764 / .3797	
Fuel Injection Stagnation Pressure Ratio	.945	.90	.85	.941	.888	.835	.94 / .941	.88 / .885	.83 / .883	2 Shocks / 3rd Shock
Oblique Detonation Stagnation Pressure Ratio	.155	.0854	NA	.108	.0688	.0549	.0583 / .0887	.0663 / .0855	.0461 / .0616	
P_{05}/P_{01}	.137	.0716	NA	.108	.0523	.0392	.0419 / .0317	.0663 / .0855	.0461 / .0616	

NA - Detonation Wave is Detached

ϕ - Equivalence Ratio

Table 8.5.1 Performance of the $\Theta = 5^0$ Reflected Shock Hydrogen-Air Oblique Detonation Wave Ramjet

	$M_1=6$ 12.9% Spillage			$M_1=8$			$M_1=10$			
	$\phi=1/3$	$\phi=2/3$	$\phi=1$	$\phi=1/3$	$\phi=2/3$	$\phi=1$	$\phi=1/3$	$\phi=2/3$	$\phi=1$	Remarks
C_T Ideal	.23	.40	.59	.14	.26	.38	.09	.18	.26	Uncorrected for f/A
C_T Uncorrected F/A	.144	.32 .279	NA	.11	.20	.28	.059	.14	.20	Corrected for Spill at $M_1=6$
C_T Corrected F/A	.155	.303	NA	.121	.223	.316	.069	.162	.234	
I_{sp} Ideal	A700	4400	4100	3900	3700	3500	3300	3150	3000	
I Uncorrected F/A	3200 3787	3400 2961	NA	2800	2800	2900	2400	2500	2400	Corrected for Spill at $M_1=6$
I Corrected f/A	3000	3216	NA	3080	3122	3273	2807	2893	2808	
Diffuser-Shock Stagnation Pressure Ratio	.913	.913	.913	.859	.859	.799	799	799	.799	
Fuel Injection Stagnation Pressure Ratio	.0095 .943	.019 .890	.0285 .840	.0095 .941	.019 .88	.0285 .834	.0095 .94	.019 .88	.0285 .827	
Oblique Detonation Stagnation Pressure Ratio	.205	.146	NA	.210	.104	.074	.181	.0936	.0658	
P_{05}/P_{01}	.176	.119	NA	.170	.0786	.0530	.136	.0658	.0430	

NA - Detonation Wave is Detached

ϕ - Equivalence Ratio

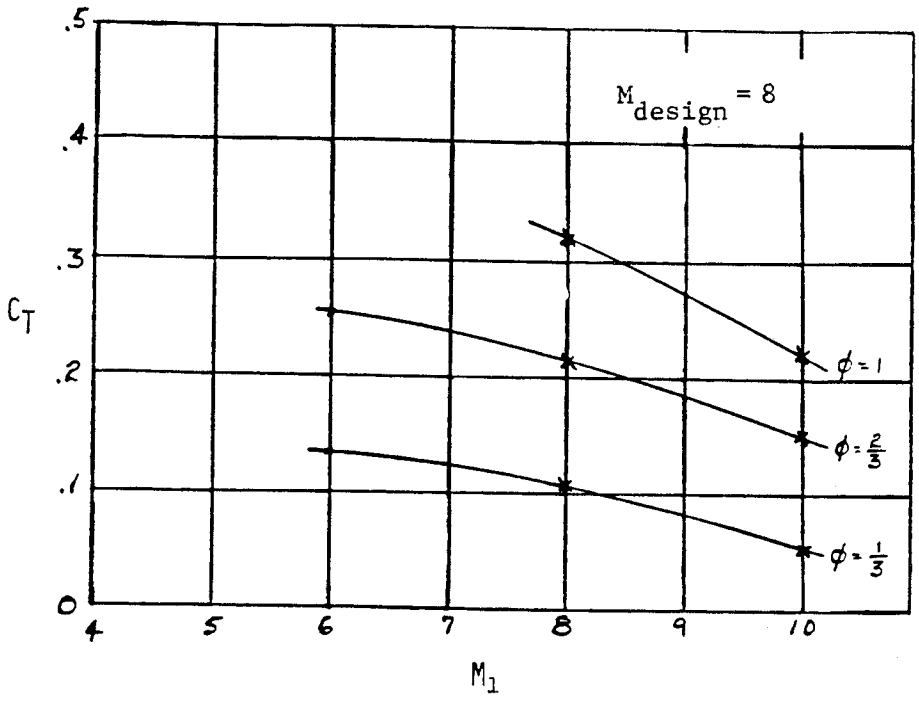

Figure 8.4.1 Thrust Coefficient of the Multiple Shock Diffuser Oblique Detonation Wave Ramjet

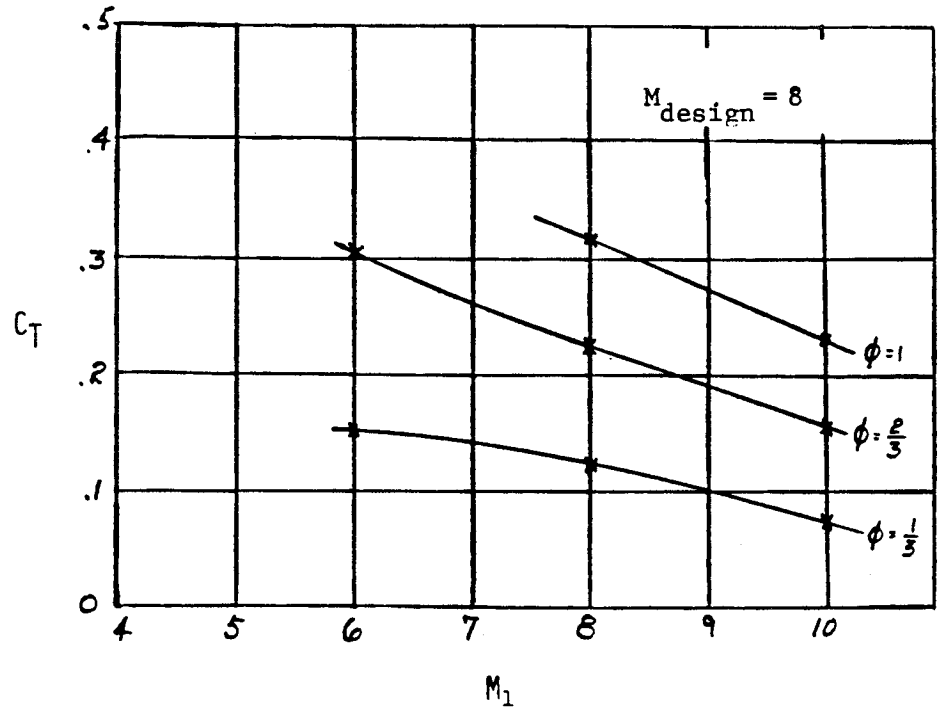

Figure 8.5.1 Thrust Coefficient of the Reflected Shock Diffuser Oblique Detonation Wave Ramjet

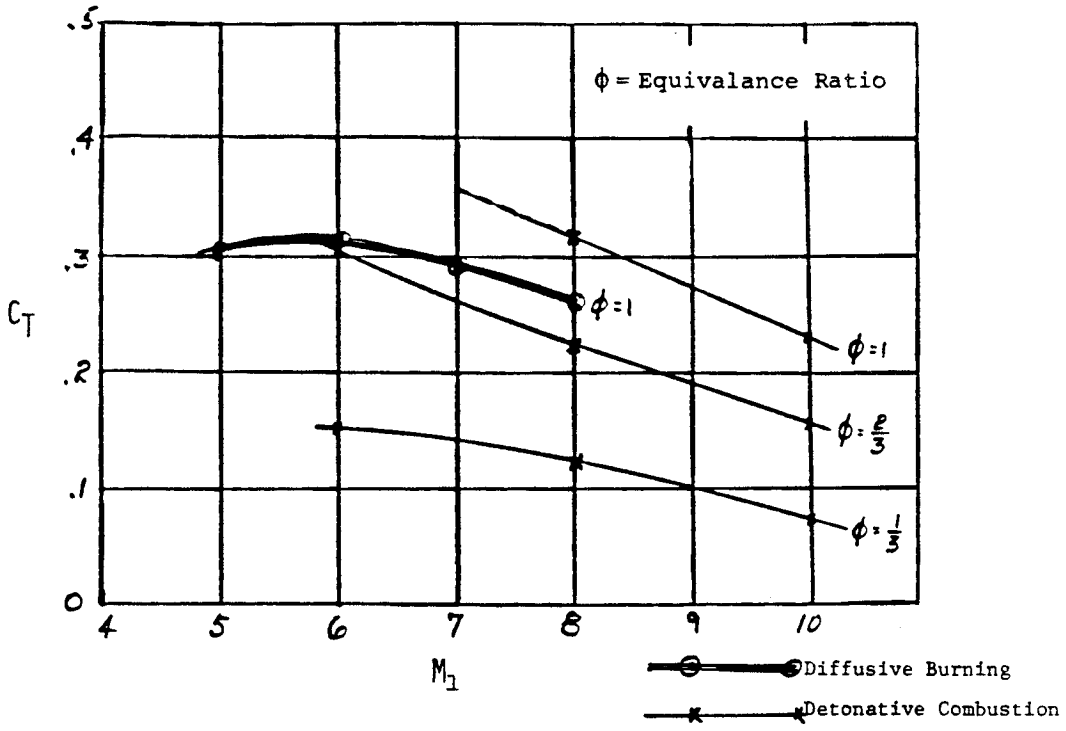

Figure 8.6.1 Thrust Coefficient Performance Comparison of the Reflected Shock Oblique Detonation Wave Ramjet with the Diffuser Burning Scramjet

9.0 Conclusions

The oblique detonation wave ramjet offers great potential as an airbreathing propulsor to extend the range of the ramjet flight Mach numbers from takeover speeds of $M_1 \cong 6$ to $M_1 \cong 14$.

Steady-state ramjet operation at flight Mach numbers in excess of $M_1 = 6$ poses many problems of aerodynamic heating/cooling/heat transfer that may well be insurmountable for long periods of sustained flight circa 10 to 20 minutes. It is also questionable that any mission exists that requires sustained flight at these high flight numbers.

The use of the ramjet, however, in accelerated flight provides a means of attaining high boost phase velocities for launch vehicles with specific impulses that are approximately an order of magnitude superior to the chemical rocket. Problems of aerodynamic heating/cooling/heat transfer would be largely alleviated for this mode of operation.

The potential of the oblique detonation wave ramjet appears to be most applicable to ramjet operation in accelerated flight, otherwise the high flight Mach number performance capabilities would be masked by the aerodynamic heating/cooling/heat transfer problems. Airbreathing propuslion systems are the means by which future launch vehicle technology must progress.

Universal Systems, Inc.
Arlington, Virginia
August 31, 1979

10.0 REFERENCES

1. Adamson, T. C., and Morrison, R. B., "On the Classification of Normal Detonation Waves," Jet Propulsion, August 1955.

2. Patch, Richard W., "Prediction of Composition Limits for Detonation of Hydrogen-Oxygen-Dilutent Mixtures," ARS, 14th Annual Meeting, Washington, D. C., November 1959.

3. Schott, G. L., and Kinsey, J. L., Kinetic Studies of Hydroxyl Radicals in Shock Waves, II, Induction Times in the Hydrogen-Oxygen Reaction, J Chem. Phys., Vol 29, No. 5, November 1958.

4. Huber, P. W., Schexnayder, D. J., Jr., and McClinton, C. R., Criteria for Self-Ignition of Supersonic Hydrogen-Air Mixtures, NASA Technical Paper 1457, August, 1979.

5. Morrison, R. B., and Ingle, M. J., Design Data for Aeronautics and Astronautics, Aeronautical & Astronautical Engineering Department, the University of Michigan, Library of Congress Catolog card number 61-71267, John Wiley and Sons, Inc. July 1961.